UNIVERSITY OF NAIROBI

DEPARTMENT OF PHYSICS

FIRST PRINCIPLES CALCULATIONS OF STRUCTURAL, ELECTRONIC, MECHANICAL AND OPTICAL PROPERTIES OF K_2SbAu PNICTIDES TERNARY SEMICONDUCTOR
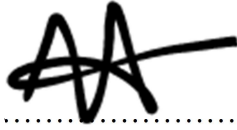
BY

MUSANYI IBRAHIM

I56/39018/2021

A Thesis Submitted in Partial Fulfilment of the Requirements for the Degree of Master of Science in Physics of the University of Nairobi.

SEPTEMBER, 2023

DECLARATION

I declare that this thesis is my original work and has not been submitted to any other University. Where other people's work has been used, this has properly been acknowledged and referenced per the University of Nairobi's requirements.

Signature: ……………………………………. Date…………………3/9/2023………

Name: Musanyi Ibrahim, Reg No: I56/39018/2021

Department of Physics, Faculty of Science and Technology

This research thesis is submitted for examination with our approval as research supervisors;

Prof. Robinson J. Musembi

Department of Physics, University of Nairobi, P.O Box 30197-00100 Nairobi

musembirj@uonbi.ac.ke

Signature: …………………………………………..Date: ………3/9/2023………….
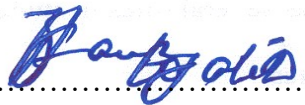
Prof Francis W. Nyongesa

Department of Physics, University of Nairobi, P.O Box 30197-00100 Nairobi

fnyongesa@uonbi.ac.ke

Signature: …………………………………..Date: …3/9/2023……..

DEDICATION

To my beloved parents and the entire family for the priceless support, inspiration and guidance

To the University of Nairobi for the award of scholarship

ABSTRACT

The most active research currently in the field of semiconductors is the determination of the most efficient materials for application in photovoltaics and optoelectronics. Semiconductors compounds have attracted great attention, and the most interesting type is the ternary semiconductors whose potential has not been fully realized. The work being reported here studied the structural, electronic, mechanical, elastic and optical properties of K_2SbAu pnictide ternary semiconductor.Density functional theory (DFT), a first-principles method, was employed to compute the structural, electronic, elastic and optoelectronic properties. Ground state structural properties were obtained using the generalized gradient approximation exchange-correlation potential with ultrasoft Perdew-Burke-Enzerhof (PBE) and Perdew-Burke-Enzerhof for solids (PBEsol) as the exchange-correlation functionals. Another functional used was the Perdew-Zunger for the Local Density Approximation (LDA) exchange-correlation potential. The equilibrium lattice parameters were the key structural properties of the material derived from the computed equation of state (EOS). Moreover, mechanical stability was tested on elastic constants which were obtained to be 6.60149Å for GGA , 6.19105 Å for LDA and 6.39519 Å for PBEsol. The deduced direct band gaps were obtained from the calculations as 0.9430 eV, 0.9060 eV, and 0.8482 eV for PBE, PBESol and LDA, respectively. In all cases, Au-$3d$ orbitals were observed to be dominant at the top of the valence band. Lastly, frequency-dependent optical spectra were calculated with the aid of microscopic dielectric tensors. The optical properties were calculated as refractive index, absorption coefficient, energy loss, and reflectivity. The K_2SbAu material optical bandgap on average was found to be 2.5 eV, suggesting that it can be a potential for solar photovoltaic applications.The results obtained were in agreement with the experimental values for structural properties, and this investigation should trigger further research interests to broaden the knowledge base on these materials from a theoretical perspective.

TABLE OF CONTENT

Table of Contents

LIST OF FIGURES

LIST OF ABBREVIATIONS/ ACRONYMS AND SYMBOLS

DFT   Density Functional Theory

DOS   Density of states

FP-LAPW   Full-Potential Linearized augmented plane wave

GGA   Generalized Gradient Approximation

LDA   Local Density Approximation

LEDs   Light-emitting diodes

QE   Quantum Espresso

SC   Semiconductor

PDOS   Projected Density of States

PBE   Perdew-Burke-Ernzerhof functional

LDA   Local Density Approximation

GGA+U   Generalised Gradient Approximation with Hubbard U correction

$\alpha(\omega)$ Absorption coefficient

$n(\omega)$ Refractive index

$R(\omega)$ Reflectivity

$L(\omega)$ Energy loss

(EPM)   Empirical Pseudopotential method

FPAW   Full Potential Augmented Wave

$V_{ion}\,,\,U(\vec{r})$ Local and non- local potential

K-S   Kohn-Sham theorem

$V_s\,(r)$ Local external potential

$\check{T}_s(n)$ Kinetic energy

$E_H(n)$ Hartree -energy

$E_{XC}(n)$ Exchange- correlation energy functional

$V_{eff}(r)$.   Effective potential energy

PAW   Plane augmented wave function

B_o Bulk modulus

CB   Conduction band

VB   Valence band

B_H Hill approximation for bulk modulus

G_H Hill approximations for shear modulus

N_{VR} Poisson ratio

K_2SbAu potassium antimony and gold based pnictide ternary semiconductor

ACKNOWLEDGEMENT

CHAPTER ONE: INTRODUCTION

1.1 Background to the Study

Semiconductors are widely used in electronic devices such as integrated circuits, diodes, LEDs, transistors, solar cells, electronic/electrical actuators, and sensors. Because of their related optoelectronic qualities spanning from narrow to wide bandgap and high electrical conductivity, compound semiconductors have seen tremendous device development (Pan and Zhu, 2015). For example, group III-V compounds such as gallium arsenide (GaAs) can be used in several optoelectronic devices such as in telecommunications in optical fibre, solar cells, and infrared detectors/sensors, among others (Mokkapati and Jagadish, 2009). Semiconductors are tuned to produce various groups of intermediate binary or ternary semiconductors in order to gain features suitable for diverse uses. The crystal structure of a compound semiconductor material is made up of elements which may possess ordered and or disordered atomic phases that are substituted in the parent structure as illustrated in figure 1 (Pan and Zhu, 2015).
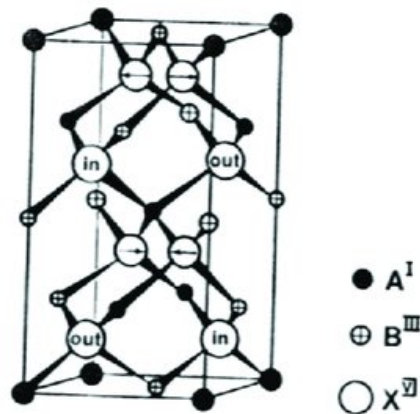
Figure 1.1: Parent structure of zinc blende crystal structure (Peter *et al*, 2005)

Pseudo-binary alloys are also known as ternary semiconductor alloys and are formed by combining the anions of AC and BC which are a constituent of two binary semiconductors.

The resulting material compounds take the form $A_{1-x}B_xC$ commonly known as ternary semiconductors. It is assumed that the cations are randomly distributed in the respective fcc sublattices where $A_{1-x}B_xC$ represents a cation-substituted alloy (Bell, 2018).

Compound semiconductors are categorized as binary, ternary, and quaternary, and their alloys are known as pnictide ternary semiconducting materials (Peter *et al*, 2005). These materials, specifically pnictide semiconductor compounds, have diverse applications in several areas such as nuclear energy, optoelectronics, thermoelectricity and magnetism (Boublenza *et al*., 2021). Semiconductor radiation detectors require compounds that can withstand extremely high temperature and pressure conditions, thus compound semiconductors are more suitable compounds since they have a large atomic number with a corresponding higher density (Boublenza *et al*., 2021).

Ternary ABC_2-type semiconductors are categorized into two groups; one group consists of A^{I} B^{III} C_2^{VI} named ternary chalcopyrite compounds. This group are alloys of binary and their isoelectronic frame forms the group II-VI binary compounds (Jaffe and Zunger, 1984). Therefore, the binary compounds have similar properties to that of group II-IV-V2 pnictide ternary semiconductor (John, 2007). However, ternary chalcopyrites are $CuGaS_2$, $CuInSe_2$, $AgInS_2$, etc (Hao *et al*., 2014). These compounds have been theoretically studied extensively due to their unique features and wide range of applications (Mallmann *et al*., 2019).

For the Grimm-Somerfield rule, the conductivity for such semimetal compounds is deduced by the systematic replacement of groups II and IV by group III (Koitabashi *et al*., 2010). The name given to group II compounds is ternary pnictides which contain A^{II} B^{IV} C_2^{V} constituent elements. The resulting material compounds exhibit similarity with group III-V compound (Boublenza *et al*., 2021).

However, compounds such as $CdGeP_2$, $CdSnAs_2$ and $ZnSiP_2$ are pnictide ternary semiconducting materials (Jaffe and Zunger, 1984). Regarding their crystal geometry, they are generically similar to the ternary structure of zincblende (Martins and Zunger, 1985).

Chalcopyrite ternary pnictides have become an interesting area of concern for many researchers as a result of their unique structural, mechanical, optoelectronic, and vital physical properties such as melting point, a high index of refraction and nonlinear susceptibility among others

(Chen, 2013). These materials therefore form potential raw materials for solar energy, and thermoelectricity (Es-smairi *etal.,* 2022).

There is a lack of both experimental as well as theoretical studies of K_2SbAu pnictide semiconductor material in the literature however there exist similar compounds studied in the literature having the same properties. K_2SbAu pnictide material is mechanically stable and has a narrow band gap that matches the solar U-V spectrum. This makes it a potential candidate for optoelectronic application. Thus, this work analyses the structural, electronic, mechanical and optical properties of K_2SbAu using the Density Functional Theory approach.

1.2 Statement of the Problem

Ternary pnictide semiconductors' mechanical and optoelectronic characteristics have been studied. Pnictide ternary semiconductors have been the subject of several theoretical and experimental studies, but little is known about their optoelectronic characteristics. The main driving force behind this research is the fact that, despite the presence of other compounds with comparable properties, the K2SbAu compound has received comparatively little experimental and theoretical attention. The current theoretical computation investigations will lay the foundation to further theoretical and practical research on the K2SbAu compound in the future. Due to the stability under the mechanical stress of K2SbAu, it is important to investigate the viability of using it in optoelectronics applications. In this work, the structural, electrical, mechanical, and optical properties of the pnictide ternary semi-conductor compound K2SbAu are revealed, and prospects for optoelectronic applications are investigated.

1.3 Objectives
1.3.1 Main Objective

To perform first-principles calculations of structural, electronic, mechanical and optical properties of K_2SbAu pnictide ternary semiconductor

1.3.2 Specific Objectives

1. To study the structural and electronic properties of K_2SbAu pnictides ternary semiconductor

2. To investigate the mechanical properties of K_2SbAu pnictides ternary semiconductor

3. To determine the optoelectronic properties of K_2SbAu pnictides ternary semiconductor

1.4 Justification and Significance of the Study

Semiconductor materials play an important role in the optoelectronic industry where such materials find a wide range of applications. Among the chalcopyrites, the chalcogenides have received a lot of attention more than the pnictides and to this juncture, many of the pnictides remain less studied despite their potential for application in the optoelectronic industry. Theoretical study on pnictide ternary semiconductors reveals structural, electronic, optical, and mechanical properties of the material essential for optoelectronic applications. Therefore, since the K_2SbAu compound has similar properties as the existing ternary compounds and there is no literature reporting on the same, hence makes it worth for study. This research work will be useful in future experimental and theoretical investigations. These will explore more potential of K_2SbAu compounds for optoelectronics applications and hence provide more knowledge for reference. The outcome of the research will serve as an upgrade for pnictide ternary semiconductors in the fields of optoelectronics.

1.5 Scope of the study

The structural, electronic, mechanical and optoelectronic properties of K_2SbAu are studied using the first-principles computational method (DFT), The work is arranged in the order as indicated; Chapter one deals with the introduction of Semiconductors, types of ternary semiconductors and various applications. Chapter two gives a detailed review of the literature on related materials. Chapter three gives the theoretical framework scope.

Chapter four gives an elaborate methodology. Chapter five provides work results with a discussion of the obtained data in comparison to different approximation methods used. Chapter six provides conclusions and recommendations and future gaps.

CHAPTER TWO: LITERATURE REVIEW

2.0 Introduction

Currently, many body interaction problems in material science are being solved by Computational methods. The method is able to control inventions and examine new but complex material for research (Knauth, 2002). The method's applicability benefits numerous disciplines like solid state physics and quantum chemistry thus being an interdisciplinary approach. For a better understanding of detailed knowledge of this technique, simulation approaches are vital and have led to a greater impact on material designers who benefit fully from the computations method. The technique has been used to bridge the gap between theory and experiments hence providing an alternative to interrogating a vast range of materials. The results obtained forms a basis for future research reference.

2.1 Semiconductors and their Alloys

In solid-state physics, materials are classified as metals, semiconductors, and insulators. The semiconducting materials can be further classified in terms of their electrical conductivity and energy bandgap range. This classification states that a semiconductor's electrical conductivity ranges from 10^{-9} -10^2 S/m while the energy band gap lies in the range of 0 to 6 electron volts (eV) (Adachi, 2017). Some materials have small energy gaps such as silicon and Germanium while others have large band gaps such as Zinc Sulphide (ZnS) and Diamond (Adachi, 2017). The elements or compounds with overlapping valence and conduction bands have no band gaps and therefore are termed metals, while those with large band gaps are considered insulators (Sturge, 2020).

Studies characterize materials to possess either direct or indirect bandgap semiconductors according to the types of band structures (Chen, 2013).

Technological advancement in semiconductor alloys attracts the most attention because of the tunability of optoelectronic properties such as the bandgap through varying alloy compositions (Peter *et al*, 2005). Optoelectronic device applications depend on the materials' energy band gaps and their abilities to conduct electricity either by use of electrons as the majority of the charge carrier or hole (Peter *et al*, 2005).

Basic alloys such as Ge_xSn_1 and Si_xGe_{1-x} are compounds formed by two groups of five elements in the periodic table (Guevara *et al*., 2007). Ternary alloys take the form AB_xC_{1-x} and are determined by replacing some atoms B in basic compound(binary) AB with C atoms which are usually in the same group as B in the periodic table (Chen and Dongguo, 2013). These compounds have been theoretically and experimentally studied and hence act as the reference point. Similarly, the synthesis of alloys that are quaternary in nature has been experimentally done, where the replacement of atoms is done by other atoms from the neighbour columns of the periodic table (Koitabashi *et al*., 2010).

2.2 *Narrow Band Gap Alloys and their Applications*

Material alloys whose bandgap is termed narrow are those whose bandgap is smaller than silicon (Chen and Ravindra, 2019). The band gaps of such alloys are found in the infrared region. The ranges of wavelength for infrared categorizes into near, mid and far-infrared ranges as 0.78-3 µm , 3-50 µm and 50-1000 µm(Chen and Ravindra, 2019). The narrow bandgap, for such compounds as GaAsSb and HgCdTe are useful in thermoelectric and detection by infrared radiation (Rogalski, 2005).

Among the narrow bandgap semiconductors, the GaAsSb system allows the operation of bipolar transistors which are heterojunction that operate in a frequency of terahertz range (Rogalski, 2005). The lining up of bands that stagger in the GaAsSb/InP is an example which not only launches electrons at the collector with high initial energies but also eliminates the problem of electron blocking (Chen and Ravindra, 2019). However, GaAsSb can be used in place of traditional THz application material as it is grown at low temperatures. The narrow bandgap field in semiconductors of II-VI group dominates in applications such as solar devices (Hegedus and McCandless, 2005).

The main infrared material has a wide bandgap which covers all infrared regions with varying compositions. Secondly, there is no change in variation of the composition as depicted by the lattice constant. Lastly, the direct bandgap of the material allows a hundred per cent efficiency due to its large coefficient of absorption(McCandless, 2005).

Additionally, its low thermal noise allows high-performance detectors which results from long minority carriers making the highest operating temperature detectors (Peter *et al,* 2005).

Previously, researchers have investigated chalcopyrite-type ternary semiconductors which have unique properties for thermoelectric properties both theoretically and experimentally (Fan *et al*., 2017). Results from theoretical studies have shown the maximum power factor of p-type $AgInTe_2$ as 0.91 and $AgGaTe_2$ as 1.38 at a temperature of 800K. While efficiency ZT is up to 0.22 at 675K (Fan *et al*., 2017). The group I-II-VI semiconductors known as ternary alloys have been extensively researched (Es-smairi *et al*., 2022). The researchers have revealed thermoelectric and optoelectronic properties that ensure such compounds are key in the application of optoelectronic and photovoltaic devices (Es-smairi *et al*., 2022).

2.3 Wider band gap of the semiconductor alloy

The alloys termed semiconductors are said to have a wide band gap if the energy gap is beyond 2.5eV. Therefore such compounds experience extensive application as a result of their ability in conducting electricity and field break down (T.D.Moustakas, 1992). In many research done on semiconductors, wider band gap semiconductor has contributed immensely since various materials possess such properties and are readily available for study.

Group III-V nitrides have a wide band gap. Thus, most scientists have focused on it as an interesting area of immense concern, due to their applicability in photodetectors and light-emitting diodes. The advantage of such a photodiode is that dark current is minimum as a result of having a large potential barrier. Moreover, it regulates quantum efficiency as the thickness of

the intrinsic layer is controlled. With such applications related to wider-gap semiconductors, many technological developments have been initiated in improving the existing devices.

Materials that possess wide band gap semiconducting properties have numerous range of applications in developing and fabricating solid state devices which are technologically important.

For instance, ZnS_xTe_{1-x} compounds and like ZnS_xSe_{1-x} are essential in developing devices useful in various spectral regions because its constituent has direct band gaps in the range over 2.75eV (Haase *et al*., 1991). Some of the semiconductors can be transformed and matched to produce wonderful technological advancements such as blue light-emitting diodes and lasers.

2.4 Solar Cells Application

The alloys of semiconductors have important applications in Solar cells (Al., 2016). So far the leading material that is abundant with high conversion efficiency is silicon thus suitable for solar cell production (Al., 2016). However; the use of silicon materials in the solar cells industry is hindered by the fact that silicon solar cells are economically unfavourable (Hegedus and McCandless, 2005). This is because of their high cost of production resulting from the high temperatures required to extract silicon from its earth occurrence. Ternary pnictide semiconductors are the latest alloy that most researchers have shifted focus on due to their good structural, electronic and optical properties. This enables them to be a potential candidate for optoelectronic usage (Irfan *et al*., 2021).

2.5 Optoelectronic Properties

The ternary semiconductors crystallize to form a chalcopyrite structure that is tetragonal in nature (Beloš *et al*., 2013). Such ternary compounds are widely studied as potential materials for applications in nonlinear optical devices and photovoltaic cells (Sheng *et al*., 2018). K_2SbAu is an example of a ternary material in which many important properties are not yet known.

The dielectric constants of the material compute other spectral properties which are key for optoelectronics applications (Koitabashi *et al*., 2010).

With the real dielectric constant we are able to deduce a number of optoelectric properties, that is, coefficient of absorption, energy loss, material's reflectivity constant, and refractive index which are expressed mathematically as indicated in the equations(C.kittle, 1996).

With equations, one can easily fix in the expression with obtained data from the dielectric constants hence computing optical properties which are essential in optoelectronic applications

$$\alpha(\omega) = \sqrt{2}\omega \left(\sqrt{\varepsilon_{re}^2(\omega) + \varepsilon_{im}^2(\omega)} - \varepsilon_{re}(\omega) \right)^{\frac{1}{2}} \quad 1.2$$

Absorption coefficient α(ω),related with real and imaginary part of dielectric constant expression

$$n(\omega) = \left(\frac{\sqrt{\varepsilon_{re}^2(\omega) + \varepsilon_{im}^2(\omega)} + \varepsilon_{re}(\omega)}{2} \right)^{\frac{1}{2}} \quad 2.2$$

Refractive index of the material n(ω),expressed as an equation

$$R(\omega) = \frac{[\varepsilon_{re}(\omega) + j\varepsilon_{im}(\omega)]1/2 - 1}{[\varepsilon_{re}(\omega) + j\varepsilon_{im}(\omega)]1/2 + 1} \quad 3.2$$

Reflectivity R(ω),

$$L(\omega) = \frac{\varepsilon_{im}(\omega)}{\varepsilon_{re}^2(\omega) + \varepsilon_{im}^2(\omega)} \quad 4.2$$

Energy loss L(ω) expressions

2.6 Thermoelectric Properties

We can deduce materials' performance by investigating thermoelectric properties. Seebeck coefficient and power factor are important for binary alloys (Mahan *et a*l., 1997). These characterize the efficiency of the thermoelectric materials which include the ternary semiconductors (Madsen and Singh, 2006). The obtained electronic energy bands have a direct link to the Seebeck coefficient, for instance, such parameters are useful for thermal and electronic conductivity (Madsen and Singh, 2006).

Seebeck constants was obtained which depend on relaxation time and the BoltzTraP code was a fundamental tool for deducing the parameters (Yousuf and Gupta, 2019). Thermoelectric defines the ability of a material to aid in the re-use of heat energy produced to useful electrical energy which researchers are concerned about (Yang, 2005). Thus, the energy crisis problem can be addressed by studying and proposing materials with good thermoelectric properties.

In establishing the relationship among various coefficients of transport properties, the material's structure of band at the high symmetry zone of Brillouin and density of states are employed.

See beck coefficient with many other abilities of a material to conduct both thermal and electrical, thermoelectric scientific scenario is developed. The Seebeck coefficient variation shows the n-type behaviour of heat carriers.

2.7 Empirical Studies on Semiconductors

Most crystal structures for ternary semiconductors are related to that of zinc-blende binary structure but with tetragonal strain parameters (Shiyou et al., 2009). In this case, group five II-IV-V_2 chalcopyrite-structure and electronic properties calculations are reported for such semiconductors (Jaffe and Zunger, 1984).

The trends in their properties also involve the distribution of charge, bonding and band structure that were analysed from the chemical composition of the compound (Jaffe and Zunger, 1984).

The clarity of the zinc 3d orbitals and their role is also clarified for such group five II-IV-V$_2$ compounds. Additionally, the structural distortion and bonding together with the band gaps of the zinc-blende parent crystal structure of ternary compounds were investigated.

In addition, the optical and electronic characteristics of Cu$_2$ZnGeSe$_4$and Cu$_2$ZnGeTe$_4$ quarternary semiconductor structures have been studied which depicts characteristics similar to ternary with variation of band gaps and the nature of curves obtained (Shiyou *et al*., 2009).

Material's reflectivity, coefficient of absorption, refractive index, and dielectric function were studied for such compounds hence useful knowledge in interpreting bandgaps of material classified under pnictide ternary semiconductors.

The interband transitions assigned by optical spectra form critical points that are calculated as per band structure. Thus, the behaviour of such properties concerning the structure of the crystal and anion atoms were investigated qualitatively (Jaffe and Zunger, 1984).

Recently authors described an ab-initio study on chalcopyrite's compounds of group I-III-VI$_2$ makes the Empirical Pseudopotential Method (EPM) difficult. In these studies, the calculations were extended to the ternary pnictides structure of group II-IV-V2 semi-conductor compounds (Jaffe and Zunger, 1984).

The ordering in the structure of ternary systems was studied with the same functional and results obtained (Hao *et al*., 2014). Such similarity between groups of semiconductor alloys was found to be thermodynamically preferred (Hao *et al*., 2014).

The most recent research done on this related compound was the first-principles calculation, on two newly designed ABC$_2$ ternary pnictides semiconductors. Where structural, optoelectronic, and mechanical properties of the named compounds, K$_3$Cu$_3$P$_2$ and K$_3$Ni$_3$P$_2$ were studied (Irfan *et al*., 2021).

The properties were obtained theoretically by an ab initio study, which was used in the most accurate FPAW and modified BJP (Irfan *et al*., 2021). The exchange interactions and electronic correlation in compounds K$_3$Cu$_3$P$_2$ and K$_3$Ni$_3$P$_2$ were accounted for, as employed in GGA together with GGA + U method, respectively (Fan *et al.,* 2017).

These compounds were found more stable and hence could be synthesized. The band structure was calculated and the nature of semiconductor nature identified with band gap values of order 1.7 eV and 1.82 eV were predicted.

In summary, from the review of the previous work done on pnictide ternary semiconductors, it can be deduced that pnictide ternary semiconductors are useful for mechanical and optoelectronic properties. Even though, there is insufficient literature on the studies of K_2SbAu pnictide ternary semiconductor material, similar compounds with sufficient literature are available for comparison.

Thus, this study seeks to solve the gap in knowledge by studying for the first time it's structure, electronic, optical and mechanical properties of K_2SbAu using DFT for potential applications in mechanical and optoelectronic fields.

CHAPTER THREE: THEORETICAL FRAMEWORK

3.1 Introduction

Material properties can be best described in terms of interactions within an electronic system. The system's contents are atoms which form the basic component of matter. In performing *ab initio* calculations of materials, structural and electronic properties are important aspects of material sciences (Sholl and Steckel, 2011).

The condensed matter properties depend on the electrons and nuclei of the materials by providing necessary knowledge about the structural, electronic, mechanical and optoelectronic properties of various materials (Salah Daoud *et al*., 2019). Many studies are ongoing on many-body system theories, which involve the solution of the fundamental equation, the Schrödinger equation. The equation is such that there is interaction between the system's electrons and the external Coulombic field. For instance, the interaction occurs as a result of atomic nuclei and other fields from outside the atom (Schrödinger, 1926).

3.1.1 The Schrödinger Equation

The properties of matter are described from theoretical methods by starting with Hamiltonian for N electrons and P nucleus for the interacting systems. The Hamiltonian explicit equation takes the form of **equation 5.3** below.

$$\hat{H} = -\frac{\hbar^2}{2m_e}\sum_{i=1}^{N}\nabla_i^2 - \sum_{I=1}^{P}\sum_{i=1}^{N}\frac{Z_i e^2}{|R_I - r_i|} + \frac{1}{2}\sum_{j\neq 1}^{N}\sum_{i=1}^{N}\frac{e^2}{|r_i - r_j|} - \sum_{I=1}^{N}\frac{\hbar^2}{2M_I}\nabla_I^2 + \frac{1}{2}\sum_{I=1}^{P}\sum_{J\neq I}^{P}\frac{Z_I Z_J e^2}{|R_I - R_J|}$$

Where R and r are nuclear and electron coordinates respectively. The fundamental constants are plancks constant ℏ, mass of electron m and electron charge e. H is the Hamiltonian operator,

while Ψ is a set of Eigen states or solutions for the Hamiltonian, and each has an associated eigenvalue E_n which satisfies the Eigen equation (Sholl and Steckel, 2011).

The wave function Ψ, for many-body systems, relies on the nucleus in the system and the position of each electron (Gidopoulos and Gross, 2014). The electrons are denoted by *i* subscript while nuclei are denoted by *I* subscript with their corresponding charges and mass of nuclei.

The general Hamiltonian equation can be thus simplified to take the form of equation 6.

$$\hat{H} = \check{T}_n + V_{nn} + \check{T}_e + V_{en} + V_{ee} \qquad\qquad 6.3$$

The first term $\check{T}_n$ in equation 6 indicates the kinetic energy of the nuclei N of the system, while V_{nn}, which is the second term, stands for potential energy as a result of repulsion among the nuclei.

$$\check{T}_n = -\sum_{I=1}^{N} \frac{\hbar^2}{2M_I} \nabla_I^2 \qquad\qquad 7.3$$

$$V_{nn} = \frac{1}{2}\sum_{I=1}^{P}\sum_{J\neq I}^{P} \frac{Z_I Z_J e^2}{|R_I - R_J|} \qquad\qquad 8.3$$

The other terms represent electronic kinetic energy as well as electronic potential energy which result from electrons-nuclei interaction energy and electron-electron interactions.

Equation 9 represents electronic kinetic energy.

$$\check{T}_e = -\frac{\hbar^2}{2m_e}\sum_{i=1}^{N} \nabla_i^2 \qquad\qquad 9.3$$

Equation 10 stands for electronic-nuclei interaction potential energy

$$V_{en} = -\sum_{I=1}^{P}\sum_{i=1}^{N}\frac{Z_i e^2}{|R_I - r_i|} \qquad 10.3$$

Equation 11 represents electron-electron repulsion potential energy

$$V_{ee} = \frac{1}{2}\sum_{j\neq 1}^{N}\sum_{i=1}^{N}\frac{e^2}{|r_i - r_j|} \qquad 11.3$$

3.2 Density Functional Theory

The energy at the ground state for many-electron systems is represented as a function of its electron density. The ground-state electron density can, therefore, be obtained by first calculating the ground-state energy by minimizing the total energy of the system (Sholl and Steckel, 2011). Therefore, instead of solving the many-electron wave function, N non-interacting electrons with the same ground-state density are considered, and energy $E(n)$ is minimized to yield the ground-state density $n(r)$ (Sholl and Steckel, 2011).

Given the complexity of interactions between the electrons and nuclei, several approximation methods have been used. Among them is the Born-Oppenheimer Approximation, which gives a separate treatment to the electrons and nuclei of an atom.

3.2.1 Born-Oppenheimer Approximation

The Born-Oppenheimer approximation decouples electrons and nuclei into separate mathematical problems (Spohn and Teufel, 2001). Thus, the full-wave functional is given by this number of electrons multiplied by the corresponding 3-dimensional problem when solving it.

Oppenheimer Approximation states that the wave function of electrons relies on the nuclei's position R_I but not velocities, which means the motion of nuclear is slower than electrons i.e. treated as fixed (Peter *et al.*, 2005). For any particle in the interacting system, its motion is a unique function of all other particle's motion hence solutions of the Schrödinger equation become more complicated prompting various approximations.

$$\left[\sum_i^N \frac{p^2}{2M_1} + \sum_i^{ne} \frac{p^2}{2m_e} + \sum_{i>j} \frac{e^2}{|r_i - r_j|} + \sum_{i>j} \frac{e^2}{|\mathbf{R_i} - \mathbf{R_j}|} z_i z_j - \sum_{i,j} \frac{e^2}{|\mathbf{R_j} - r_i|} z_i \right] = E\Psi \qquad 12.3$$

Where r_i, r_j are the ith and jth positions of electrons. Z_i, $Z_{j\_}$ are the Ith and Jth atomic numbers of ions while R_I, R_j are the Ith and J^{th} positions of ions with their corresponding m omentum p.

The wave function for this approximation takes the form $\Psi\,(\mathbf{R_I}, \mathbf{r_i})$ and expressed as

$$R_I, r_i) = \Psi_e(R_I, r_i)\Psi_n(R_I) \qquad 13.3$$

The electron's wave function and the corresponding nucleus wave function are generated. When fitted back to equation 7 we obtain two distinct Hamiltonian equations; One for the nucleus and the other for the electron. Now since the nucleus is treated as fixed the approximation ignores it and thus the approximation reduces to electronic Hamiltonian alone as shown

$$\hat{H} = \check{T}_e + V_{en} + V_{ee} \qquad 14.3$$

In a detailed way, it can be written as shown below, where nuclear interaction is decoupled out.

$$\hat{H} = -\frac{\hbar^2}{2m_e} \sum_{i=1}^{N} \nabla_i^2 - \sum_{I=1}^{P} \sum_{i=1}^{N} \frac{Z_i e^2}{|R_I - r_i|} + \frac{1}{2} \sum_{j \neq 1}^{N} \sum_{i=1}^{N} \frac{e^2}{|r_i - r_j|} \qquad 15.3$$

3.2.2 Hartree-Fock Theory

The decoupled Hamiltonian equation for many body systems by the first approximation, Hartree-Fock theory considers that the wave function is depicted by a single state determinant of N spins-orbits. It is expressed as follows,

$$\Psi = \Phi 1(x1) \quad \Phi 1(x1) \dots \dots \Phi 1(xn)$$

$$\Phi 2(x2) \quad \Phi 2(x2) \dots \Phi 2(xn)$$

$$\Phi N(x1) \quad \Phi n(x2) \dots \dots \Phi(xn) \qquad (16.3)$$

Variable x is the electron's coordinates and φ wave function of the electron which is normalized. Substitution of φ in (3) minimizes Hamiltonian with the use of multiplier ε to φ yielding:

$$\frac{\sigma}{\sigma\emptyset}\left[< H > - \sum \in I \int |\emptyset j| 2dr\right] = 0 \qquad (17.3)$$

Further simplification yields a simpler Hartree equation which is a set of one-electron equations denoted as follows;

$$-\frac{1}{2}\Delta\emptyset i\ (r) + V_{ion}(r^{\rightarrow})\emptyset_i(r^{\rightarrow}) + U(r^{\rightarrow})\emptyset_i(r^{\rightarrow}) = \varepsilon_i\varphi(r^{\rightarrow}) \qquad (18.3)$$

$V_{ion}\ U(r^{\rightarrow})$ represents local and non-local potential respectively.

Equation (16) converts the Hamiltonian of the many-body system to several single Hamiltonian which again assumes the correlation of electrons (Sholl and Steckel, 2011). This theory yields small widths of band gaps but larger in semiconductors. Therefore, the many-body Hamiltonian equation is converted to various single-electron Hamiltonians and neglects the electronic correlations.

3.2.3 Hohenberg-Kohn Theorems

Hohenberg-Kohn is the existing simple theory that makes DFT possible. It proves that in many systems of particles that interact, the external potential is a unique function of the density and thus density is uniquely determined (Perdew *et al*., 1996). The theorem determines the many-electron system problem by the particle's density, not its motion.

Originally the theory framework was developed by Fermi and Thomas in 1927, and named as the Thomas Fermi model(Chen and Dongguo, 2013). The DFT theory was further improved by Hohenberg and Kohn through the formulation of theorems.

The first considered theorem was that the ground state energy is a special functional of the density of a particle($E_0 = E\{n(r^{\rightarrow})\}$)(Sholl and Steckel, 2011). The theorem considers correlations of an electron as compared to the Hartree theorem. Its equation is expressed as;

$$E\{n(r^{\rightarrow})\} = \mathrm{F}\{n(r^{\rightarrow})\} + \int n(r^{\rightarrow}) V_{ext}(r^{\rightarrow}) \ \mathrm{dr} \quad 19.3$$

The solution of the equation was determined by Kohn and sham who separated the second term of the equation into three distinct parts.

Hohenberg-Kohn Theorem's first theory states that potential acting externally corresponds to a functional of n(r) since external potential fixes the Hamiltonians operator. Similarly, it is rare for an electronic system to comprise of similar charge density that consists of different potentials that act upon it. Thus, such an operator (Hamiltonian) is simplified for charge density, hence used for many body problems (Manfredi, 2020).

The use of charge density can replace the tedious calculations based on wave functions by substituting the usual descriptions based on wave functions. However, there exist two major challenges in the application of this theorem;

First, there is the unknown part, which prompts us to first get it in order to obtain and fulfil the second requirement once the unknown is accepted as ground state charge distribution.

Second, the consideration of Lagrange multipliers is ignored even though it is the second part of the problem. The first part of the problem was addressed by (Kohn, 1995), as discussed in the next part,

3.2.5 Kohn-Sham Theorem

Kohn and Sham organized problems that deal with many-body system interactions into a detailed and familiar form which enhanced the practical application of DFT (Sholl and Steckel, 2011). The resulting equation generates similar density as given systems of interacting particles neglecting non-existing systems.

The K-S equation illustrates the non-interacting particles and how they freely move by a local effective potential acting externally (Sholl and Steckel, 2011). They, however, made two assumptions; first, the real exact density of state (ground) can be taken as the density of particles that don't interact. Secondly, the formed Hamiltonian consists of kinetic energy and an effective local external potential V_s (r) that acts on an electron at point **r**.

The Hamiltonian is then expressed as;

$$\left[\frac{-\hbar^2}{2m_e}\nabla_{(r)}^2 + v_s(r)\right]\Psi_i = E^{KS}\Psi_i \qquad 20.3$$

Generally, the expression for KS total energy is written as:

$$E_{ks} = \check{T}_s(n) + \int dr V_s(r)dr + E_H(n) + E_{XC}(n) \qquad 21.3$$

Where $\check{T}_s(n)$ is the kinetic energy of electronic particles (non-interacting), $E_H(n)$ Hartree-energy and $E_{XC}(n)$ is the exchange-correlation energy function (J.Griffiths, 2000). The ground state energy and particle density can only be solved by a single electron Schrödinger equation as shown in equation 22.

$E_{XC}(n)$ is known as exchange–correlation. Apart from the exchange correlation functional, the remaining terms can be written in their explicit form;

$$\left[\frac{-\hbar^2}{2m_e}\nabla^2_{(r)} + v_{KS}(r)\right]\Psi_i = E^{KS}\Psi_i \quad 22.3$$

$$v_{KS}(r) = \int \frac{n(r')}{|r-r'|}dr' + v(n) + v_{xc}(r) \quad 23.3$$

From the equation, the functional derivative of $E_{XC}(n)$ is given as shown,

$$v_{xc} = \frac{\partial E_{XC}(n)}{\partial n(r)} \quad 24.3$$

The theoretical exact solution is provided by Kohn-Sham Equations for the energy of the ground state for the interacting systems. Since the exchange-correlation functional is unknown, then the only remaining question is its form.

Initial gauze of ρ(r)

Use ρ(r) to calculate J_{eff} (r)

V_{eff} (r)=V_{eff}(r)+$\int \frac{\rho(r)}{r-r1}dr^i$+$V_{xc}$(ρ(r))

Solve Kohn-sham equation

$[\frac{h^2}{2me}\nabla_i^2 + V\text{eff}(r)]\Psi_i=_E\Psi$

Calculate new ρ(r)

ρ(r)=$\sum|\emptyset_I (r)^2|$

Self-consistent?

Yes   NO, generate a new density functional and start from initial

Solved! can now calculate energy, forces
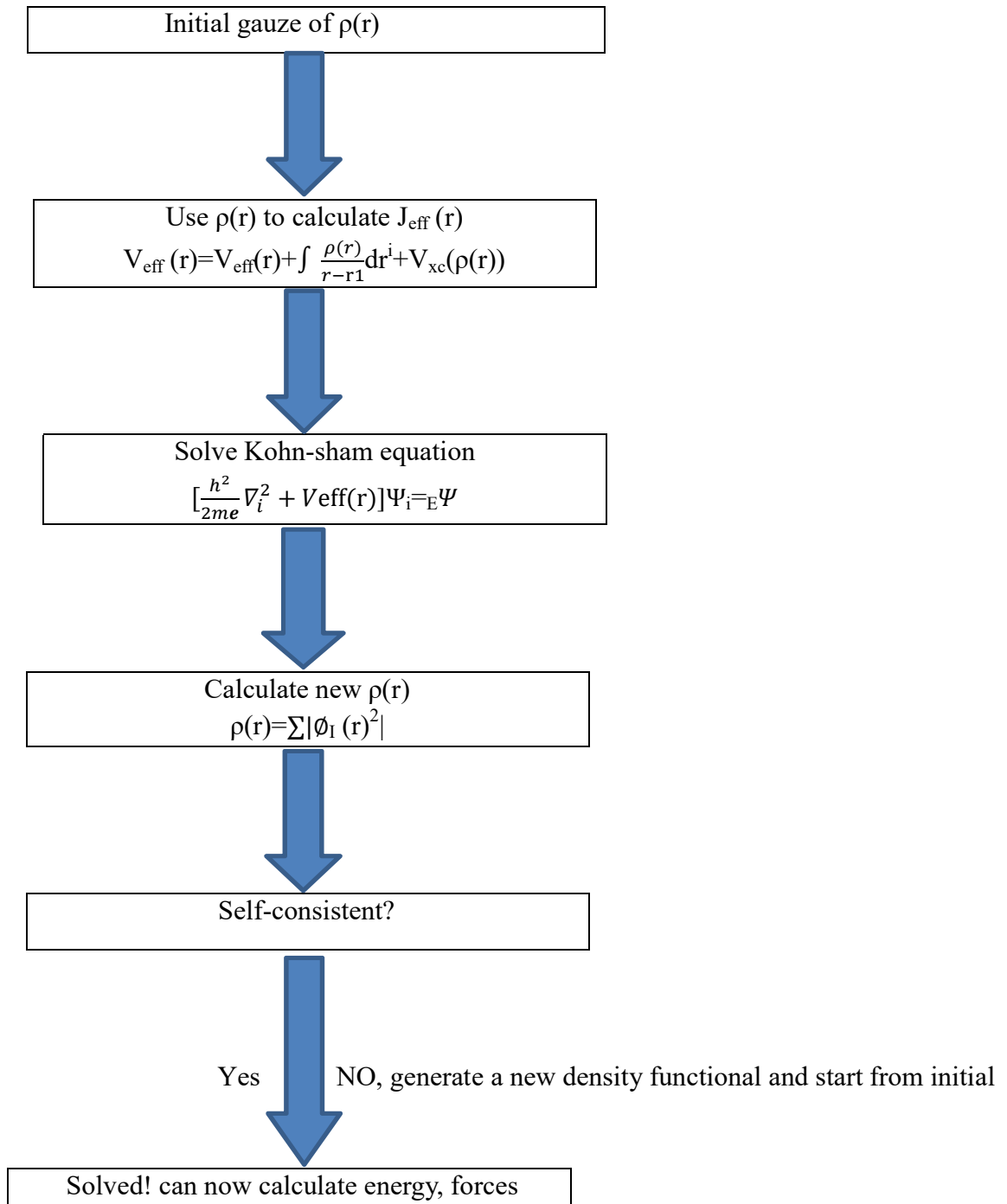
Figure 2.3: Schematic illustration of Kohn-sham solution (Sholl and Steckel, 2011)

The above illustration needs an input file of the material under study. The input consists of atoms arranged to determine the potential of an atom V(r), together with atomic number Z. Where we first gaze at charge density, Hartree potential and the calculated exchange-correlation potential (Payne *et al.*, 1992). For self-consistency to be achieved, a smaller charge density is generated as compared to chosen values. Then we can deduce the minimum energy from charge density n(r) that eventually results in the minimum energy guessed (Payne *et al.*, 1992).

The density in its computation is however used as another function in calculating Hartree potential and exchange-correlation potential. The results of $V_H(r)$, $V_{XC}(r)$ and $V_{nuc}(r)$ give the effective potential $V_{eff}(r)$.

Hence, the system's Hamiltonian is equal to $V_{eff}(r)$+K.E.

$$\hat{H}\emptyset_i(r) = \left[\frac{-\hbar^2\nabla^2}{2} + V_{eff}(r)\right]\emptyset_i(r) = \in_i \emptyset_i(r) \quad 25.3$$

3.2.6 Exchange-Correlation Functional

The only idea remaining is what form of the exchange correlation functional is unknown from the K-S theorem. Thus, in order to yield its form, we must approximate the exchange correlation functional $\boldsymbol{E_{XC}n(r)}$ and it's done with various approximation techniques such as; local Density Approximation (LDA) and Generalized Gradient Approximation (GGA), where GGAs include PBE and PBEsol functional (Perdew *et al*., 1996)

3.2.7 Local Density Approximation (LDA)

According to this approximation, the correlation functional is deduced as per the equation below,

$$\text{Exec}\{n(r^{\rightarrow})\} = \int n(r^{\rightarrow}) \in_{xc}^{hom} \{n(r^{\rightarrow})\}dr \quad 26.3$$

The term $\int \in_{xc}^{hom} \{n(r^{\rightarrow})\}$ is the exchange correlation energy for a gas of uniform density (Sholl and Steckel, 2011). On the contrary, the key challenge is that it gives inaccurate results in a system where an independent particle breakdown is required.

However, these exchange correlations in LDA can be improved when the gradient of the charge density is included, which is done in GGA.

3.2.8 Generalized Gradient Approximation (GGA)

The local density approximation provides that within the systems of interaction, density is assumed to be similar. This is unable to explain in detailed if the density increases in some molecules which in turn doesn't give a good approximation. In order to improve on this approximation, density should be taken in a way to depend on the functional and gradient of the density n(r), so as to consider the electron's true non-homogeneity that generalized gradient approximation (GGA) really introduced and formulated a detailed equation as shown.

$$\text{Exec}\{n(r^{\rightarrow}) = \int n(r^{\rightarrow}) \in_{xc}^{hom} \{n(r^{\rightarrow})\}dr + \int f[n(r^{\rightarrow}), \nabla n(r)\} \quad 27.3$$

Where the exchange correlation becomes,

$$V_{XC}^{GGA} = \frac{\partial E_{xc}^{GGA}}{\partial n(r)} = \left[\in_{xc} + n\frac{\in_{xc}}{n(r)} - \nabla(n\frac{\in_{xc}}{n(r)})\right] \quad 28.3$$

In this case, the correlation chosen, denoted by f, satisfies several known limits E_{XC}. The best way is to determine if by adjusting it to satisfy the known energy or hole for exchange correlation so as to be in agreement with the known properties. Thus, the preferred approximation is GGA since it involves the charge gradient and gives a better prediction of the results than LDA.

The GGA consists of two major categories of functional that is, Pardew-burke-Ernzerhof (PBE) functional and revised PBE functional PBEsol that improves prediction of solid properties of equilibrium.

We have used both, LDA, PBE and PBEsol in our calculations. Despite success in the wide use of these approximations, the hindrances that face them are, the unable to describe properties correctly like the electronic of some materials. Hence to deal with such limitation, a hybrid and GW functional is employed.

3.2.9 Hybrid Functionals and GW approximations

Numerous research works indicate that when analyzing band gaps using GGA and LDA, their band gaps are found to be underestimated for various materials.

 These challenges are overcome by suitable Hybrid DFT functional. This is obtained by suitable mixing DFT exchange functional both local and semi-local together with Hartree-Fock (non-local) energies in order to solve the band gaps challenges.

3.2.8 Plane Waves Basis

The density functional theory together with the Born-Oppenheimer approximation shows relations that exist by interactions of electrons and nuclei. The generated scenario becomes a problem as it requires finding solutions for many systems that interact. For the single-state particle problem, the particle is in motion with an existing effective potential with nuclei that are taken to be stationary. To execute the calculations, the systems are expanded into a set of plane waves so as eigenstates for the homogeneous electron are not identical to particle atoms. The expansion is fundamental for the Kohn-Sham wave function as it is useful during energy calculations of the solid. The solution obtained is for the Schrödinger equation and must therefore obey Bloch theorem.

The theorem can be expressed as $e^{ik.r}$ and a lattice periodic function u_k(r) k denoting a wave vector within the Brillouin zone (C. Kittle, 1996).

$$\psi_k(r) = e^{ik.r} u_k(r) \hspace{6cm} 29.3$$

The lattice periodic function is given by an expression;
$$u_k(r+R) = u_k(r) \hspace{6cm} 30.3$$

Substitute in the equations above, we get;

$$u_k(r) = \sum_G cGke^{iG.r} \qquad\qquad 31.3$$

Where G is a reciprocal lattice and G.b=2πm, b is the translator vector of the crystal lattice.

$$\psi_k(r) = \sum_{k,G} C_{k,G} e^{i(K+G).r} \qquad\qquad 32.3$$

Thus by inserting the plane wave expression into the K-S equation, we obtain

$$\sum_G \left[\frac{\hbar}{2m} |K + G| \sigma_{GG'} + V_{KS}^{\sigma}(G - G') \right] = \in_i C_{i(K+G')} \qquad\qquad 33.3$$

We set the plane wave energy cut-off E_{cut}

$$\frac{1}{2}|K + G|^2 < E_{Cut} \qquad\qquad 34.5$$

The discrete set of plane waves describes the k-points which are an expansion of electronic wave functions, Bloch's theorem does it. It merges state (electronic) numbers at the infinite problem to finite. By computing electronic state numbers uniquely, it is possible to represent k-points according to plane waves. We only do that if the k-point and electronic state are close, hence can solve infinite mathematical calculations.

3.2.9 K-Space and Brillouin Zone

DFT calculates systems with periodic atoms in space and knowledge in materials research. The cell that periodically repeats itself is called the supercell and contains atoms. In identifying these cells, important lattice vectors are denoted. To analyze Schrödinger equations for a system that obeys Bloch theaorem,the solutions of the wavefuction is written;

$$\psi_k(r) = e^{ik.r} u_k(r) \qquad\qquad 35.3$$

The independent solving of the Schrödinger equation for varieties of values of k is attributed to Bloch's theorem. The theory creates simple and easier mathematical concepts. The DFT calculations for such theory are solved with respect to k than r, and done in a simple and easier (Sholl and Steckel, 2011). The fundamental ideas behind the expansion of e^{ikr} expression were to obtain plane waves.

The plane wave calculations are essential as it allows the use of the Fourier transform in representing real and vector space (Sholl and Steckel, 2011).

k- Space, contain a minimum volume that consists of all information of the material. For reciprocal lattice vectors, we can express it as are Wigner-Seitz cell, it is also demonstrated in real space. The Brillion zone is merely Cells in *k* space. The calculations are then based on these K-points.

3.3.0 Pseudo-Potential

The interaction of the system's surroundings can be best described by the atomic potential V(r). Every atom for instance contains valence and core electrons, between the two which are necessary for bonding.

Thus, the pseudo-potential chosen is capable of handling only valence electrons as results lower the cost of computation in the calculation.

The core electrons are treated fixed and thus eliminated and the remaining valence electrons wave function are merged and thus an illustrative description of merged pseudo-potential is shown.
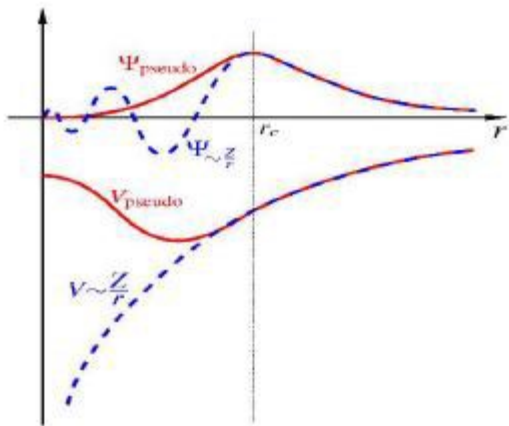
Figure 3.3: pseudopotential of an atomic wave function

The figure 3 indicates the fixed core, and the smooth node-less function is the replaced wave function. The merged Pseudo-wave function is indicated by the right arrow, and it matches all

electron wave functions. Similarly, it can be seen at a different cutoff radius that the efficient calculations using DFT are attributed to the pseudopotential chosen.

The valence state has a certain cutoff radius for every approach used (Sholl and Steckel, 2011). To produce a similar density of the charges, the electron valence regions must contain a merger of true potential and pseudopotentials applied. It has maximum displacement squared wave which is similar to potential and needs greater cut-off energies to work hence known as norm-conserving.

The ultrasoft one makes use of true pseudopotential that are matched at electron valence area, thereby reducing cut-off energies drastically. For effective performance, an orthonormality factor is employed that softens pseudo-wave functions and yields better results in the core region.
For PAW, its calculations work on the fact that the augmented plane wave and that of pseudopotential are joined and the core electrons are shallow and treated as it is. We employed the PAW and ultrasoft pseudopotentials in the predictions of various properties of the material under study.

CHAPTER FOUR: COMPUTATIONAL METHODS

4.1 Materials

In this study, a computer with an installed Quantum Espresso (QE) package was used to perform the DFT simulations. The PW and THERMO_PW drivers were installed in QE. Additionally, data visualization software including Xcrysden, Grace, Gnuplot, VESTA and Python was also used. The heavy calculations were run at the Center for High-Performance Computing (CHPC) cluster workspace in South Africa via remote access.

4.2 Methods

The first principles calculations in this work were employed as per the theory of density functional theory where the exchange correlation functionals were approximated by generalized gradient approximation and local density approximation as implemented in the Quantum Espresso code. The process started with the installation of the Quantum Espresso package together with all the other sub-software and drivers. The crystal structure of the K_2SbAu material was downloaded from the materials project website in CIF format. Materials cloud input generator in QE was used in making the PWscf input file. All the pseudopotentials for K_2SbAu material both Norm-Conserving, ultrasoft and projected Augmented wave were downloaded from the QE pseudopotential library. This study employed, PBE+ GGA, PBEsol and LDA exchange-correlation potentials.

The basic and simplest functional is the local density approximation LDA, in that the correlation energies and exchange of electron density at a point in space are estimated by a homogenous electron gas with similar density(Skelton *et al.*, 2015). However, the approximation work from a fortuitous cancellation of errors for some systems, but it does not give better results. The improvement can be done on LDA by including the density gradient, $\nabla n(r)$, which is the basis of the semi-local generalized-gradient approximation (GGA) functional. GGA functionals tend to yield improved energetics and lengthen bonds, thereby increasing cell volumes and lattice constants and softening phonon frequencies(Skelton *et al.*, 2015).

The phenomenological overbinding is corrected by GGA functionals as exhibited by the LDA, and in so doing, lattice constants values are way below the actual hence invoking the use of PBE to solve the problem of underestimations in the functional(Sholl and Steckel, 2011).

Such measures led to an improvement to the earlier PW91 GGA. In the process, good analyses of material properties are done by use of GGA and its unique function PBEsol.

4.2.1 Self-Consistent Convergence Tests

Convergence of total energy with cutoff energy, k-points and cell dimensions was performed using the input file generated from the materials cloud in order to ensure that DFT calculations and exact solutions converged.

For electronic structure, all calculations were done using the Quantum Espresso package as implemented by DFT. The calculations were based on pseudopotentials and a plane wave basis set. Thus in describing the exchange correlations effect and electron exchange, we used two different functionals: the local density functional (LDA), and the Generalized Gradient Approximation (GGA) as parametrized by Pardew Burke Ernzerhof PBE (Perdew *et al.*, 1996), PBEsol. The energy convergence criteria for this study was set at $5 \times 5 \times 5 \times 1 \times 1 \times 1$ for k-point mesh, and for cut-off energy for self-consistence calculations and the plane wave basis was set at 150Ry K_2SbAu ternary compound, with minimum varying from 60Ry-70Ry for different approximation functionals, and optimized convergent test were used in the calculation.

The calculations for this DFT theory need a lot of computational effort; thus a mathematical integration of equations is unable to occur over the *k* space entirely. Thus Pack and Monkhorst came up with a solution for this problem, Considerations of k space grid points were done, and a supercell was used that contain cubic lattice constants which is similar to k points applied.

The graphical optimized k-points graph for the two functions was obtained, Convergence of total energy with k-point Mesh curve was plotted and obtained for generalized gradient approximations by Pardew Burke, GGA+PBE.

4.2.2 Structural Properties of materials

Various structures are exhibited by different materials which are classified by numerous features in general. They are however categorized in terms of atomic structure that involves invisible features. These features are the type of bonding between the atoms and their arrangement. Secondly, micro-structure is features visible by microscopic devices for instance the microscope. They however affect the thermal, optical, electrical, magnetic properties and physical aspect of the material. The two, that is, micro and macro-structures affect elastic properties involved by the material under study.

Illustrating the properties of the materials provides an avenue to knowing metal's strength, useful in the engineering world that enhances its applicability in the discipline(Manjula *et al.*, 2016). The material's atoms are vital for understanding the structure of a material together with its atomic arrangement.

The structural properties are very essential in understanding a solid's constituent. This thesis has computed lattice parameters for the K_2SbAu pnictide ternary semiconductor's structure. The total energies were obtained in terms of the volume of cell dimensions. Thus, obtained structural properties by the equation of state were fitted in third order derivative Birch-Murnaghan equation (Chen and Dongguo, 2013). The equation of state (EOS) knowledge is vital in both applied and basic sciences as it provides insight into the fundamental solid-state theories.

Therefore, the properties obtained are lattice constant, Bulk modulus, minimum volume, minimum energy and First pressure derivative.

4.2.3 Bulk Modulus and its Pressure Derivative

The moduli expression is as shown in equation 37, which shows variations of pressure-volume and binding energy,

$$B = -V\frac{\partial P}{\partial V} = V\frac{\partial^2 E}{\partial V^2} \qquad\qquad 37.4$$

Total binding energy E for a given material in terms pressure P of the unit cell can be deduced as;

$$P = -\frac{\partial E}{\partial V} \qquad \qquad 38.4$$

At the equilibrium point, Pressure is equal to zero.

Thus the material's elastic properties are computed for bulk system and described by compressibility constant K_0,

Thus in the 37 and 38 equations, the equilibrium bulk modulus is given by (Chandra and Kholiya, 2015),

$$\frac{1}{K_0} = B_0 = -V\frac{\partial P}{\partial V} = -v\frac{\partial^2 E}{\partial V^2}]_{v=VO} \qquad \qquad 39.4$$

And its pressure derivative theoretically is defined as (Chandra and Kholiya, 2015),

$$B_0' = \frac{\partial B}{\partial V}/_{p=0} = \frac{1}{B_0}\left(V\frac{\partial}{\partial V}\left(V\frac{\partial^2 E}{\partial V^2}\right)\right)_{v=vo} \qquad \qquad 40.4$$

The Murnaghan equation is written as:

$$\Delta E(v) = E - E_0 = B_0 V_0 + \left[\frac{V_o}{B_o} + \frac{1}{1-B'_o} + \frac{V_o^{-B_o}}{B'_o(B'_o-1)}\right] \qquad \qquad 41.4$$

Where E_0 and V_o are the equilibrium energy and volume at zero pressure, B_o is the bulk modulus; B_0' is the first pressure derivative of materials (Chandra and Kholiya, 2015). These calculations are derived in terms of interatomic interactions.

Therefore the nature of fundamental solid-state theories gives can be used to determine thermodynamic parameters.

4.2.4 Elastic stability

In order to compute the information about the mechanical properties, elastic constants are vital. Such mechanical properties like bulk moduli, shear moduli, poisons ratio, Young modulus and anisotropy of material are computed using two approaches.

In DFT the two approaches are useful in the calculation of the elastic constants: the stress-strain approach and the energy-strain. Therefore in this research, we used a stress-strain approach to calculate elastic constants as it was determined from linear fit functions, according to Robert Hooke's Law.

Thus the given energy density is in the form,

$$U = \frac{\Delta E}{V_o} = \frac{1}{2}\sum_i^6 \sum_j^6 C_{ij}e_i e_{ji} \qquad\qquad 42.4$$

Where ΔE is the energy increase from the strain with vectors $e_i e_{ji}$, basically, the C is a matrix space for elastic constants(Chandra and Kholiya, 2015). Bulk elastic properties include the bulk modulus B and shear modulus G which were calculated using Voigt-Reuss-Hill averaging schemes(Hill, 1952).

For a crystal with an orthorhombic structure, bulk modulus for Voigt averaging $\mathbf{B_v}$ and the Voigt shear modulus $\boldsymbol{G_v}$ are defined as,

$$B_v = \frac{1}{9}[C_{11} + C_{22} + C_{33}] + \frac{2}{9}[C_{12} + C_{13} + C_{23}] \qquad\qquad 43.4$$

$$G_v = \frac{1}{15}[C_{11} + C_{22} + C_{33} - C_{12} - C_{13} - C_{23}] + \frac{1}{5}[C_{44} + C_{55} + C_{66}] \qquad\qquad 44.4$$

Similarly, the Reuss bulk modulus B_R and Reuss shear modulus is written in the form of,

$$B_R = 1/[(S_{11} + S_{22} + S_{33}) + 2(\boldsymbol{S_{12}} + \boldsymbol{S_{13}} + \boldsymbol{S_{23}})] \qquad\qquad 45.4$$

$$G_R = 15/[4(S_{11} + S_{22} + S_{33} - S_{12} - S_{13} - S_{23}) + 3(S_{44} + S_{55} + S_{66})] \qquad\qquad 46.4$$

For Hill approximation, the bulk modulus and shear modulus are then given by,

$$B_H = \frac{1}{2}(B_v + B_R) \;;\; G_H = \frac{1}{2}(\, G_v + G_R) \qquad\qquad 47.4$$

Of course, from the equations we get the average of the two approximations for the corresponding moduli and shear.

Poisson's ratio n and Young's modulus E can also be expressed as from the equations below,

$$E_H = 9B_H G_H/(3B_H + G_H) \qquad\qquad 48.4$$

Poisson ratio n denoted by,

$$n = (3B_H - 2G_H)/2(3B_H + G_H) \hspace{3cm} 49.4$$

The shear anisotropic factor gauges how the bonding occurs between atoms in different planes. This thesis focuses on bulk elastic constants.

Thermo_pw code implements three averaging methods; these are the one that ignores uniform strain (Voigt), the one that validates uniform stress (Reuss) and the two that show constant stiffness

4.2.5 Electronic Properties

The motion of electrons in an electrostatic field produced by nuclei describes the electronic structure of a material, this field is generated when nuclei are stationary. In this regard, the wave functions and energies of the electrons best describe the electronic properties of the material. This is done by solving quantum mechanical equations. Thus vital properties deduced are the band structure, density of states and partial density of states of a material.

4.2.6 Band Structure and Band gaps

The solid's band structure can be best described by the range of energy possessed by these electrons. The associated energies of the electrons form a network of bands termed energy bands, which are forbidden bands and allowed bands. The range of energy that can either be free from the named band energies makes them a width of bands.

These widths differ from one another due to the overlap in their orbital arrangement as per the degree of atomic orbitals(Scandolo et al., 2005). The existing band gaps are categorized as direct, and indirect. The energy state at the minimum conduction band and the energy state in the valence band maximum are differentiated by momentum. Direct band gaps are depicted when k-vectors are similar. The electron's momentum and holes depict similarity in CB and VB that is an electron can emit a photon directly(Hill, 1952). For indirect, no photon can be emitted directly but passes through a state known as intermediate in order to emit momentum to the crystal lattice.
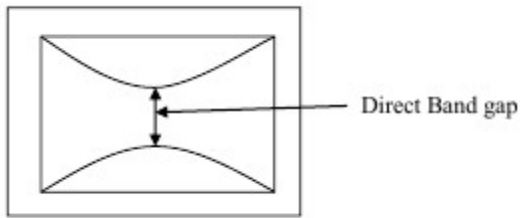
Figure 4.4 showing direct band gap
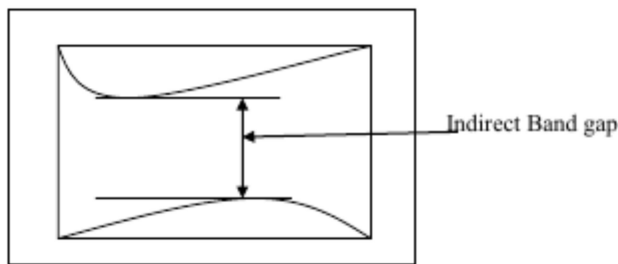
 Figure 5.4 Indirect band gap diagram of material

4.2.7 Density of States and Projected Density of States (PDOS)

The useful concept like the electronic density of states DOS which is a function of energy is vital in analyzing the solid's band structure. This is done by the use of reciprocal k-points (space) with simply the properties of the band structure. The DOS is thus illustrated as the electronic number of states in a unit volume per unit energy, an idea broadly discussed in statistical ensembles. The sum of all states within a given energy range is expressed mathematically,

$$g(\varepsilon) = \frac{2}{(2\pi)^3}\Sigma \int dk\delta(\varepsilon - \epsilon ik) \qquad\qquad 50.4$$

Where $g(\varepsilon)$ is the density of states

It can be as well be expressed in terms of fermi-energy E_f

$$g(\varepsilon) = \frac{dE_f}{d\varepsilon} \qquad\qquad 51.4$$

By normalization, we use the integral value to obtain the number of density of states N

$$N = \int_{-\infty}^{E_f} g(\varepsilon)d\varepsilon \qquad\qquad 52.4$$

Thus, the use of quantum espresso code becomes easier to compute the DOS in the above equation. By considering the contribution of an atom's existence, it is possible to compute the projected density of states PDos for every atom. In summary, states (DOS) are the domain's average space occupied by the system.

4.2.8 Electronic Transport Properties

The ab initio calculation of electronic transport properties is done on the optimized structure using the BoltzTrap theory. BoltzTrap code within the constant relaxation time approximation is carried out and obtained the required Transport Properties, the figure of merit, power factor, thermal conductivity and many more. In computing lattice thermal conductivity, the reciprocal spaces of the primitive cells were sampled. This was discussed in an earlier theoretical chapter.

4.3 Optical Properties

The components of matter in a material have constants like the dielectric constants $\varepsilon 1$, the $\mu 1$ which is represented by the charge of the field and the conductivity $\sigma 1$. Material properties such as optical for varied media need a clear and complex description of a new response function like a refractive index. The essential aspect is the association of electromagnetic waves in various media. For the occurrence of such phenomena, optical constants become fundamental in computing material's index of refraction n and the extinction coefficient k optical constants and many other properties(C.kittle, 1996).

With equations, one can easily fix the expression with obtained data from the dielectric constants and hence compute optical properties which are essential in optoelectronic applications (Ambrosch-Draxl and Sofo, 2006).

4.3.1 Reflectivity

The reflectivity can be represented as R(ω) (Ambrosch-Draxl and Sofo, 2006),

$$R(\omega) = \left| \frac{[\varepsilon_{re}(\omega)+j\varepsilon_{im}(\omega)]1/2-1}{[\varepsilon_{re}(\omega)+j\varepsilon_{im}(\omega)]1/2+1} \right|^2 \qquad\qquad 52.4$$

This equation can be reduced as,

$$R(\omega) = \left[\frac{1-N}{1+N} \right]^2 \qquad\qquad 53.4$$

$$\frac{(1-n)^2+k^2}{(1+n)^2+k^2} \qquad\qquad 54.4$$

Letting k=0, we obtain the equation below. Showing the reflectivity of the material

$$R = \left| \frac{1-n}{1+n} \right|^2 \qquad\qquad 55.4$$

If we sum over the entire conduction bands, we obtain complex imaginary dielectric functions $\varepsilon_i(\omega)$.

The absorption coefficient was also deduced since the loss of intensity per unit length is referred to as the absorption coefficient, written as

$$\alpha(\omega) = \frac{\omega}{4\pi}\varepsilon_2(\omega) \qquad\qquad 55.4$$

From the equation, we can deduce that a strong relationship between $\alpha(\omega)$ and $\varepsilon_2(\omega)$ cause an increase in high-energy absorption. Using the Quantum espresso optical program, we calculated the frequency-dependent dielectric matrix where we obtained K_2SbAu real and imaginary dielectric values. These values are fundamental in calculating the reflectivity, energy loss, absorption coefficient constants and refractive index. The curves were plotted as discussed in the analysis of the results in the next chapter

CHAPTER FIVE: RESULTS AND DISCUSSION

5.1 K$_2$SbAu Pnictide Ternary Semiconductor

In this section, the investigation results of the Face centred orthorhombic structure of the K2SbAu ternary semiconductor are presented, emphasising its structural, mechanical, electrical, and optical properties, utilizing the theoretical methodologies described in Chapter 3 and the computational details offered in Chapter 4. This section will demonstrate and discuss the results that have been achieved after a detailed analysis.

5.1.1 Crystal Structure of K$_2$SbAu pnictide ternary compound
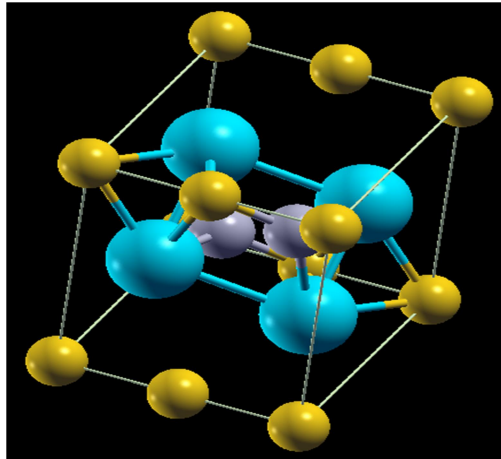
Figure 6.5: Crystal structure of K$_2$SbAu pnictide ternary semiconductor

The crystal structure was visualized using Xcrysden which is a separate software package separate from the quantum Espresso Package. The input file was generated and suitable lattice constants were 6.60149Å for GGA, 6.39519 Å for PBEsol and 6.175 for LDA. In addition, the command line for structure visualization was used for Xcrysden--input file, e.g. xcrysden -- Si.scf. in. The obtained unit cell of the K$_2$SbAu crystal lattice contains 18 atoms after performing structural optimization of the orthorhombic with relaxed structural parameters and 40 bonds covalently bonded.

5.1.2 Structure Optimization

K-Point Optimization
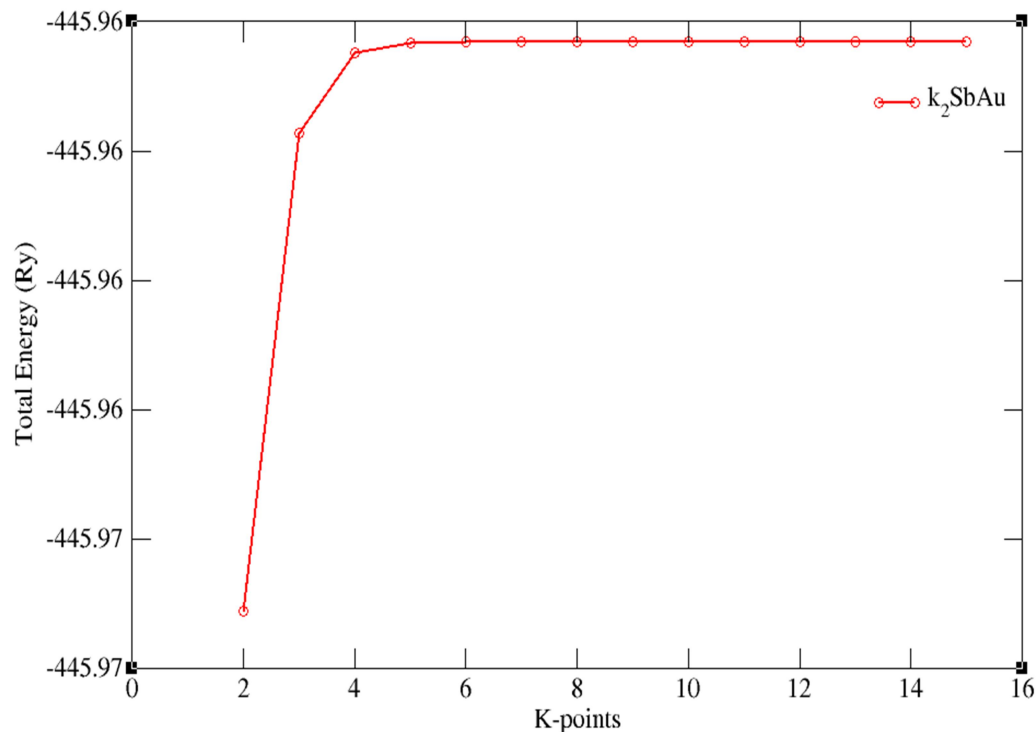
**Figure 7.5:** *K-points optimization curve using GGA for K₂SbAu*

The energy convergence with respect to the k-point was at 5 where maximum energy was attained. However, the k-point mesh here overestimated the integral computation hence the energy is too high thereby curving upwards with maximum energy approximation. As from the results, the integral numerical computation assumes the analytic form of the band energy across the Brillouin zone. Normally, most of the materials curve downwards with minimum energy approximation hence this material depicts a unique k-point optimization plot. We again, tested self-consistent convergent using pseudopotential as per parameters of PBEsol and obtained a similar k-point curve thus a proof of convergence occurring for various approximations.
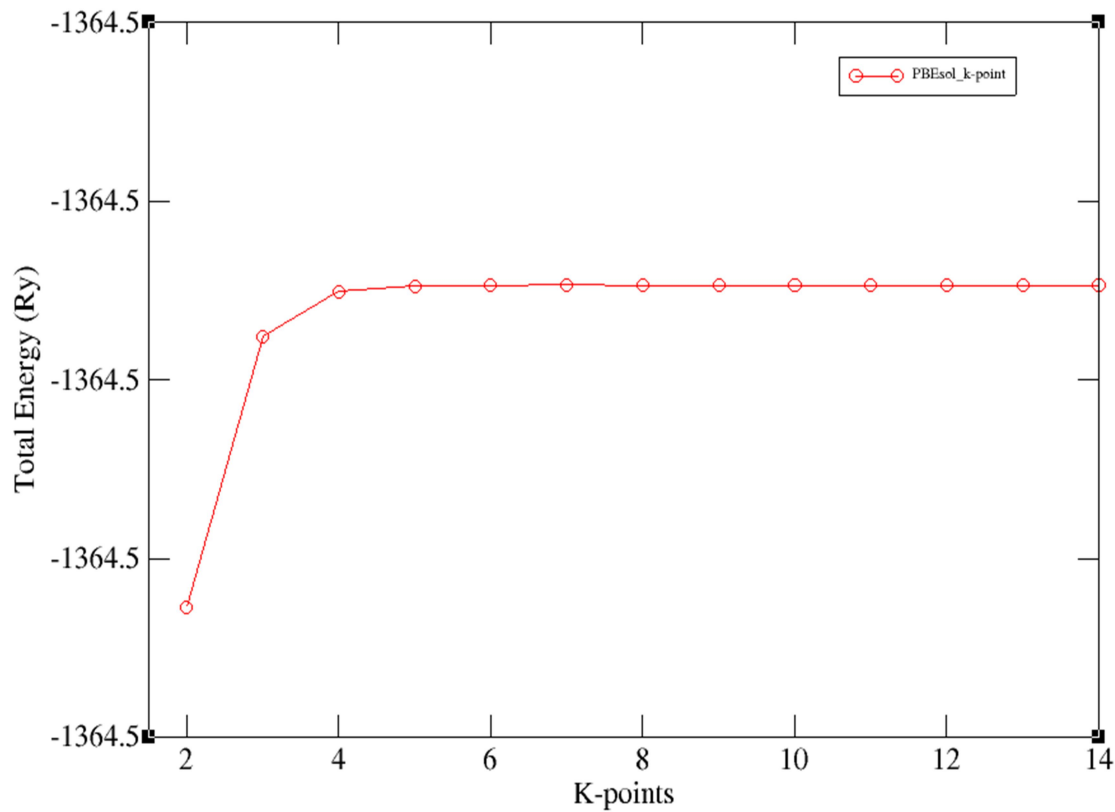
Figure 8.5: Total energy versus k-points using PBEsol.

As from the graph, the minimum total energy was obtained with k-point mesh at $5 \times 5 \times 5 \times 1 \times 1 \times 1$, and the nature of the curve is similar to that of GGA hence depicting consistent results for analysis(Chen and Dongguo, 2013). There exist slight deviations in their corresponding total energy as compared to earlier approximations, which can be attributed to differences in pseudopotentials used for varied approximation. the optimization is achieved.

Lastly, Local Density approximations functional parameters were used and tests were carried out on k-point optimization for the material under study. The parameters are the corresponding pseudopotential for the LDA of the material and its convergence test is useful to affirm that indeed the three approximations used provide similar results for other computations. The ab initio calculations were done with the converged k-point curve obtained, hence necessary to carry the involved calculations.
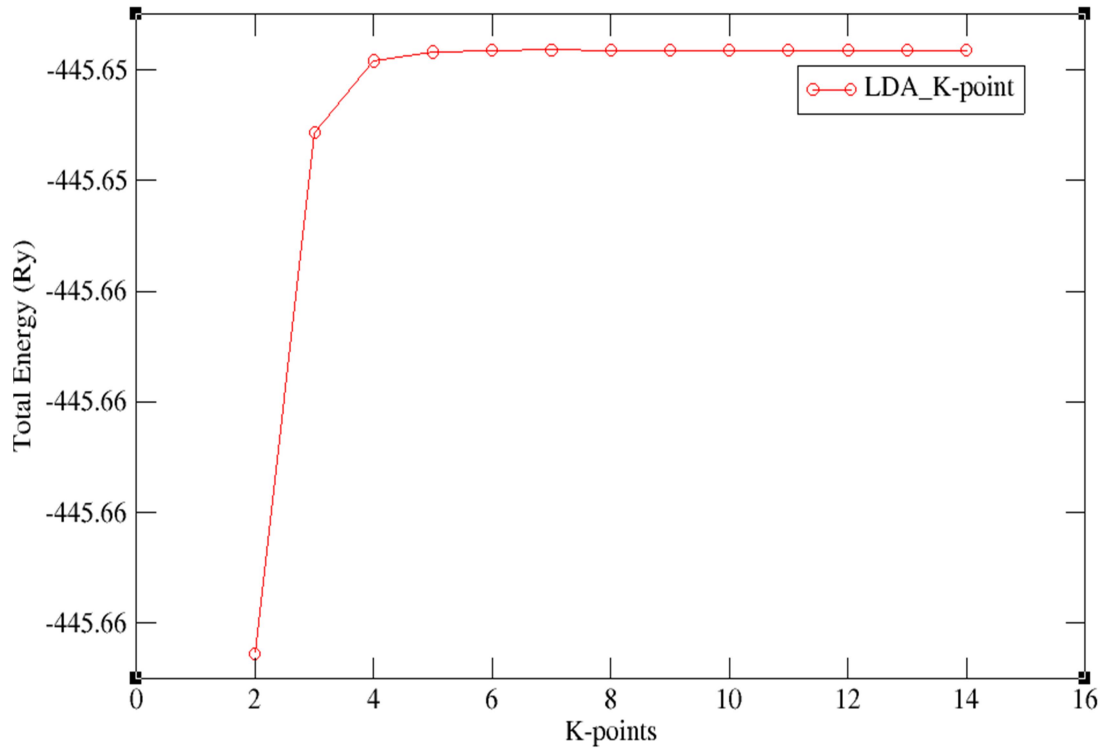
**Figure 9.5**: Total Energy against k-points mesh for LDA+PZ

The energies were underestimated even though a similar curve plot was obtained as expected from the study. However, the two approximations, are in agreement with k-point mesh convergence, which occurs at 5 5 5 1 1 1 with corresponding total energies. This is a fundamental reason to ensure that other first principles calculation to follow was done successfully. These are optimization of cut-off energy, cell dimension, and electronic and optical calculations. For cut-off energy, the test was done by use of the optimized k-points for GGA, PBEsol and LDA functional(Jaffe & Zunger, 1984).

5.1.3 Energy cut-off convergence

The related energy for plane wave plays a crucial role in the calculations performed when compounds are computed using interdisciplinary theories like density functional (Sholl and Steckel, 2011). Maximum efficiency is achieved in terms of available energy at the point of discontinuity. However, when we consider the lattice parameter and the k points, we get the expected results. When compared to arbitrarily selecting several plane waves for the basis set, this method is helpful.

An increase in energy cutoff increases the plane wave's number hence leading to an increase in the accuracy of the description of ion cores. The vital idea is to ensure energy differences remain the same since an increase in a number of plane waves does not increase charge density in the bonding. The structure's energy curve was generated as shown for K_2SbAu ternary compound using LDA, PBE and PBEsol functional. We began with PBE, and its curve optimized.

The energy convergence test for cut off energy curve was shown;
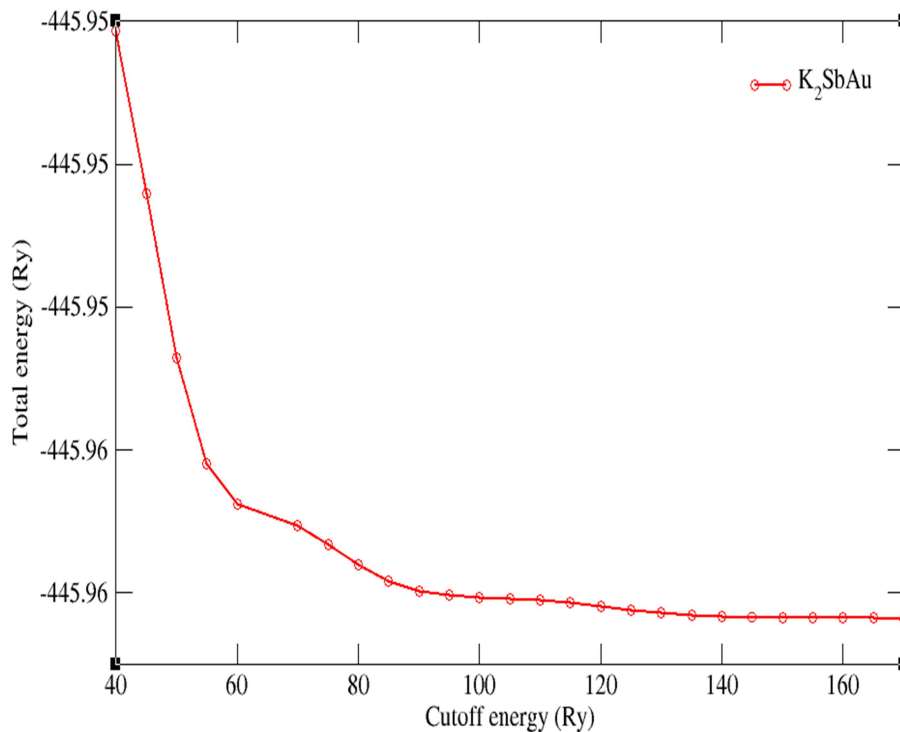
Figure 10.5*: The energy optimization plot using GGA for K_2SbAu*

The optimized energy cutoff obtained starts at 60Ry and from the graph, the best cut-off convergence energy is 150Ry for GGA of this ternary semiconductor compound. This cutoff 150 Ry together with the k-point mesh obtained becomes essential in computing the material's properties efficiently while ensuring the accuracy of the results obtained such as band structure, density of states and partial density of state.

Secondly, we set pseudopotentials for the input file of the material for PBEsol parameters and test done on cut-off energy
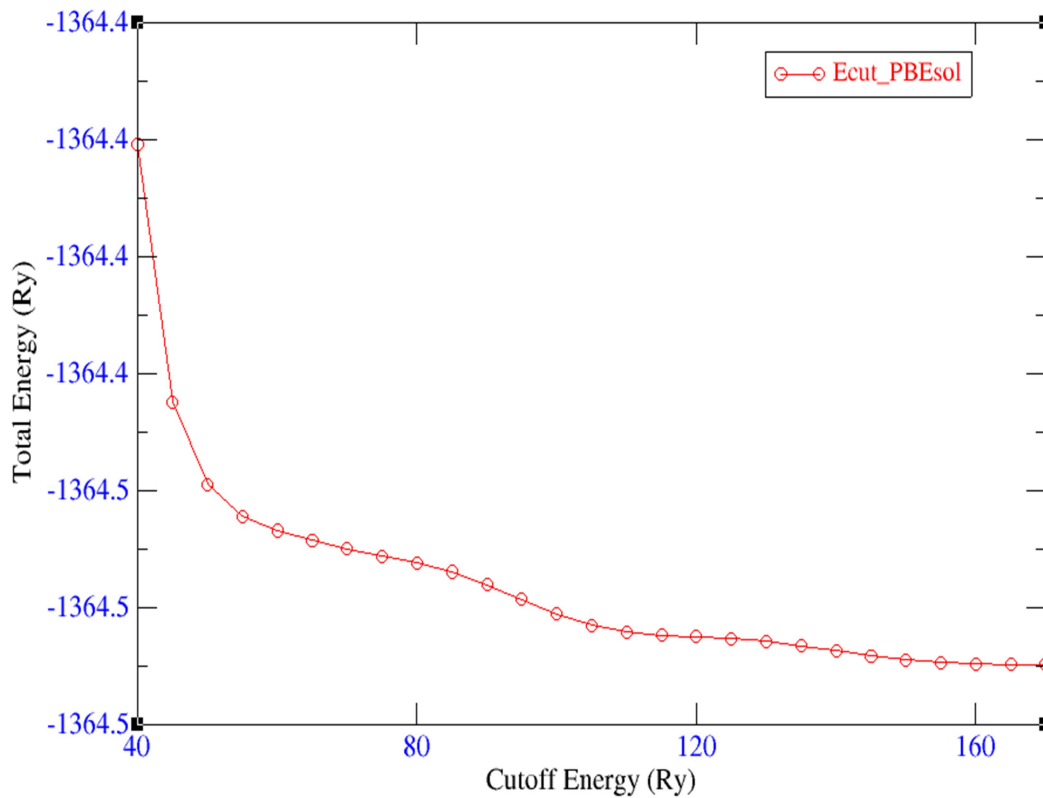
Figure 11.5: Total energy versus Cutoff Energy for PBEsol.

The initial cut-off energy began at 70Ry and still, the most useful cut energy suitable for calculation for electronic properties remained to be 150Ry.

Thirdly, LDA functional parameters were set for the cut-off energy convergence test was done and curves were obtained for the same materials.
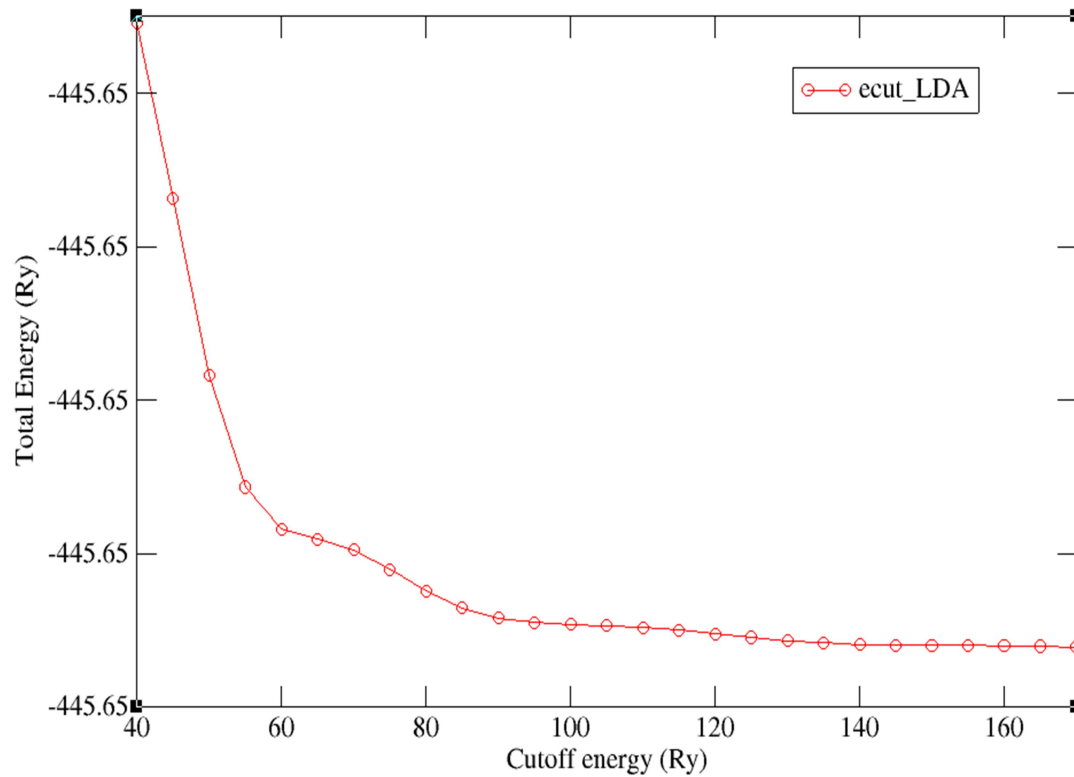
**Figure 12.5**: Total Energy versus Cutoff energy (Ry) LDA+PZ

In the entire calculation, we choose values relatively above the energy cutoff of (60Ry). These gave more accurate computational results as opposed to the minimum value from the graph. In so doing, we lower the computation cost and on the other hand, we obtain a more accurate work of calculations.

5.1.4 *Cell dimension optimization*

The cell dimension optimization provides data for detailed descriptions of the structural properties of the material under computation. Furthermore, it provides a lattice parameter necessary for other calculations, plotting this energy with respect to the volume of the lattice parameterizations; we obtain a curve that indeed depicts its convergence. The cell dimension was optimized and generated a graph showing total energy vs lattice constant.

The data obtained from optimization for both GGA and LDA was fitted in the Birch Murnagan equation of state where ground state structural properties were deduced. These properties are bulk moduli, shear moduli, Young's modulus, Poisson's ratio

Graphically, GGA provides optimized lattice constant as shown below;
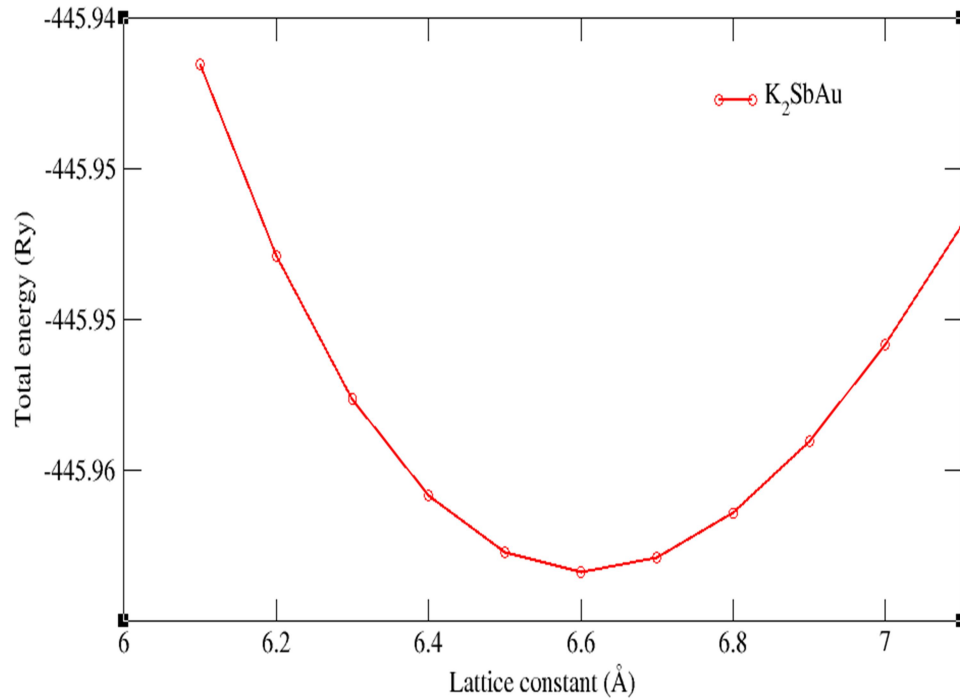
Figure 13.5: Plot for total energy versus lattice constant (GGA).

The total energy versus lattice constant plot was obtained and convergence occurred at a lattice parameter of 6.6 (A) for GGA as shown in the above plot. This in comparison with existing work of similar materials is in agreement on the nature of the curve. Thus this value was used in the calculation of electronic properties that is band structure, DOS and PDOS.

Similar curves were obtained using pseudopotentials generated from different functionals, the second one being PBEsol and lastly LDA, local density approximation.

However, the PBEsol and GGA show good general performance across all four functional employed. We generated input files using PBEsol approximation and did a cell dimension convergence test for the k-point test.
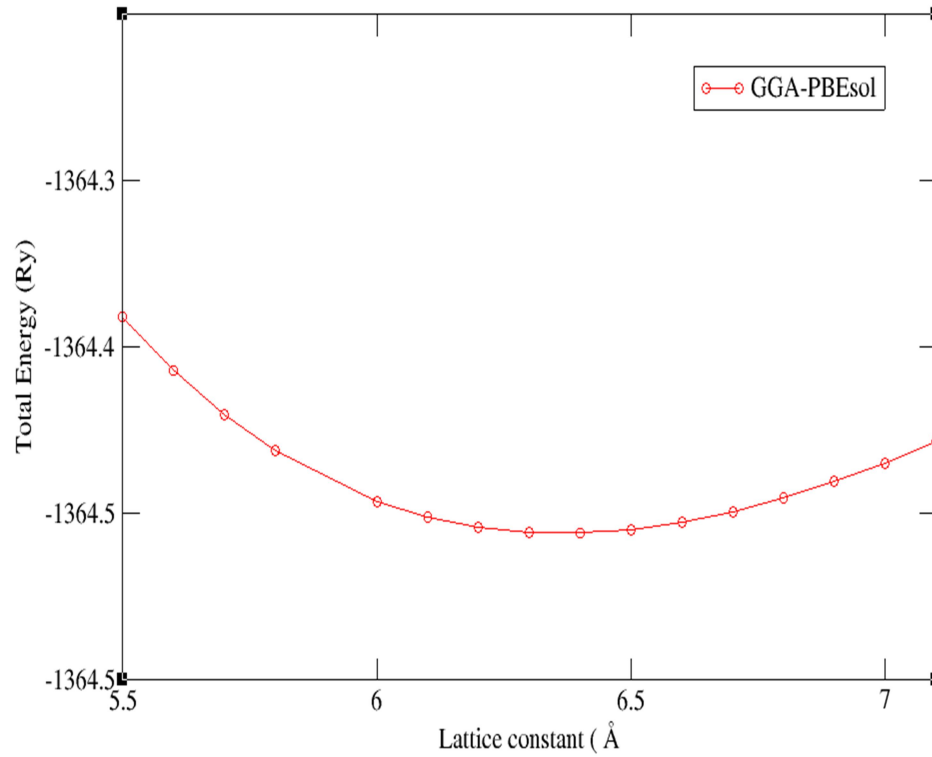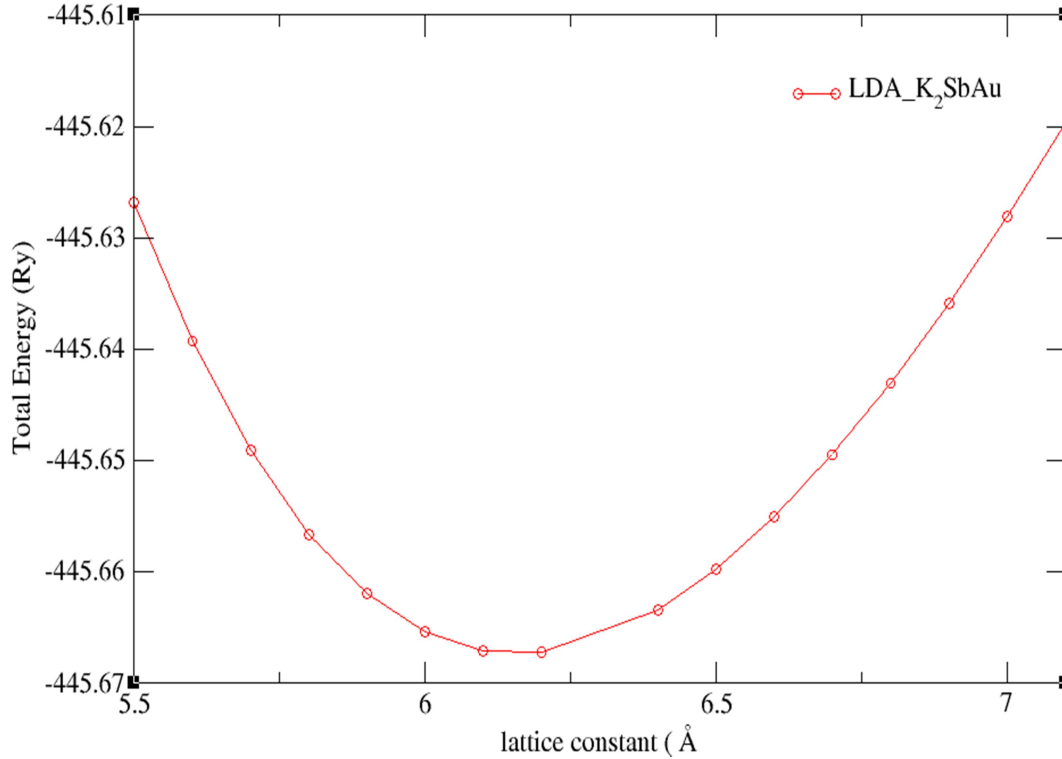
Figure 14.5: Total Energy against Lattice constant

The lattice parameter obtained as 6.39519 Å was the optimized value used in the next calculations of band structure and density of states using GGA+PBEsol pseudopotentials. The ground state structural properties were generated using cell dimension data obtained after fitting in the Murnaghan equation of state

Lastly, the Local density approximation input file was used and obtained the optimized curves for cell dimensions as shown, indicating the lattice parameters shown(Sholl and Steckel, 2011). This, just as from earlier work, we fitted in the equation of state and obtained the structural properties exhibited by the ternary pnictide semiconductor K_2SbAu.

Figure 15.5: Plot for total energy versus lattice constant (GGA).

Generally, the convergence test for k-points, cut-off energy and cell dimensions are very important in the computation of the next calculations, since these values obtained were used in structural properties and electronic. Variable cell relaxation (vc-relax) was performed to allow both variations of the atomic positions as well as lattice constants(Sholl and Steckel, 2011). The structural changes induced through relaxation including bond lengths and bond angles were determined using Xcrysden and compared with those of the original structure.

5.1.5 Structural Properties of K_2SbAu pnictides compound

These properties were obtained for various approximations used with their corresponding pseudopotential. The properties were obtained as results of fitting cell dimensions data in the equation of state for Simple cubic known as the Murnaghan equation of state within the QE package.

The material's mechanical stability was then tested through a volume optimization curve with respect to energy for K_2SbAu and plotted for various approximations.

Indeed all three approximation deduce that the compound is stable and hence possess the desired properties useful for investigation. Using the first principle FP-LAPW, the total energy was calculated for all approximations by fitting to the murnaghan's equation of state for the structural properties as represented in the tables above.

Table5.1: Ground state structural properties of K_2SbAu for GGA, PBEsol and LDA

	GGA	PBEsol	LDA
Lattice constant $(\mathring{A})$	6.60149Å	6.39519 Å	6.195105 Å
Bulk Modulus (B_o)	4.0 GPa	4.8 GPa	5.4 GPa
Min. Volume (V_o)	287.69A^3	261.55 A^3	237.30 A^3
Min. Energy (emin)	-445.95834 Ry	1364.45610 Ry	-445.6071 Ry
First pressure derivative	0.348GPa	0.234GPa	0.236GPa

Comparing the properties with respect to their approximation, it is observed that LDA underestimates the values and hence provides values lower as compared to GGA approximation(Kim *et al*., 2010).

For example from the table above we can compare their corresponding lattice parameters, GGA is 6.60149Å while LDA is 6.19105 Å. Thus, these are first-time computations of the ternary structural properties of this material. In comparison to similar compounds with the same stoichiometry like research done on compounds of K3Cu3P2 and K3Ni3P2 (S. Daoud, 2019). These compounds are both ternary pnictide semiconductors just like K2SbAu hence detailed computation brings closer correlations to their obtained results. Similarly provides the optimized lattice constants of a = b = 8.81 Å, c = 6.94 Å for Na_6ZnS4, a = b = 7.55 Å, c = 5.83 Å for Na_6ZnO4 and a = b = 9.25 Å, c = 7.12 Å for NaZnSe4(Es-smairi et al., 2022)

5.1.6 Mechanical stability

5.1.7 Elastic Properties

The elastic constants of the ternary semiconductor were calculated using GGA, PBEsol and LDA functional where it was obtained to be positive and hence mechanically stable. We also computed elastic properties and obtained the material's bulk modulus, young modulus, shear modulus and poison ratio as shown in the table below,

Table5. 2: Computed bulk modulus (B_V ,B_R,B $_H$ in GPa), shear modulus (G_V ,G_R ,G_H in **GPa**) and young modulus (E_H)

Functional	B_V	B_R	B_H	G_V	G_R	G_H	E_H
GGA+PBE	17.39	15.70	16.55	9.12	6.39	7.76	20.09
PBEsol	16.23	13.99	15.11	9.23	6.38	7.80	19.95
LDA+Pz	13.46	11.57	12.62	8.95	5.54	7.24	18.15

The bulk elastic properties are deduced using Voigt-Reuss-Hill averaging approximation for the crystal material. The value's difference depicted in the table can be attributed to the different exchange correlation functional and pseudopotential used. **B_H** is the average of bulk modulus for Voigt and Reuss approximation similar to **G_H**.

As per the criteria for brittleness and ductility of the material, the materials are categorized based on the B/G ratio. A material is said to be brittle when   B/G <1.75 while it is ductile if it is greater than 1.75.

Table 5.3: The calculated B/G ratio, Poisson's ratio (n)

Functional	B/G	n_{VR}	
GGA+PBE	2.13	0.295	present work
PBEsol	1.94	0.280	present work
LDA+Pz	1.76	0.250	present work

The GGA and PBEsol predict that the K_2SbAu compound is ductile since the ratio obtained is greater than 1.75. For LDA it underestimates the values hence the best approximation predicts that this material is ductile since the ratios 2.13 and 1.94 are greater than 1.75.

Table 5.4: The calculated independent elastic constants C_{ij} for K_2SbAu in (GPa) are as indicated in the table,

Functional	C_{11}	C_{12}	C_{13}	C_{22}	C_{23}	C_{33}	C_{44}	C_{55}	C_{66}
PBE	35.80	9.31	4.13	35.17	18.60	22.47	15.72	5.15	4.10
PBEsol	34.96	7.98	3.15	34.80	17.02	19.96	16.08	5.50	4.04
LDA	30.08	6.02	1.82	29.18	14.42	17.42	18.13	5.38	3.12

5.1.8 Electronic Properties

The properties are computed within the QE code using three approximation methods that are GGA, PBEsol and LDA. Each has a unique pseudopotential thus deducing electronic properties with some differences. The key properties are band structure, Density of State plot, and partial density of state for the K_2SbAu ternary semiconductor compound. For a better understanding of the material's properties physically, we ought to minimize energy so as to obtain the crystal's band structure.

The contained information is essential for the analysis of the band gap hence capable to predict its applicability as optoelectronic material technology. It is however noted that materials containing direct band gaps are considered active semiconductors for optical applications while those of indirect nature respond weakly to optical excitation.

. While computing band structure, the optimized dense k-point mesh used was 12× 12×12×, cell dimension of 6.6 and the ecutrho of 150Ry was employed in the calculation and thereby generating the band structure for both GGA and LDA approximation as shown below,
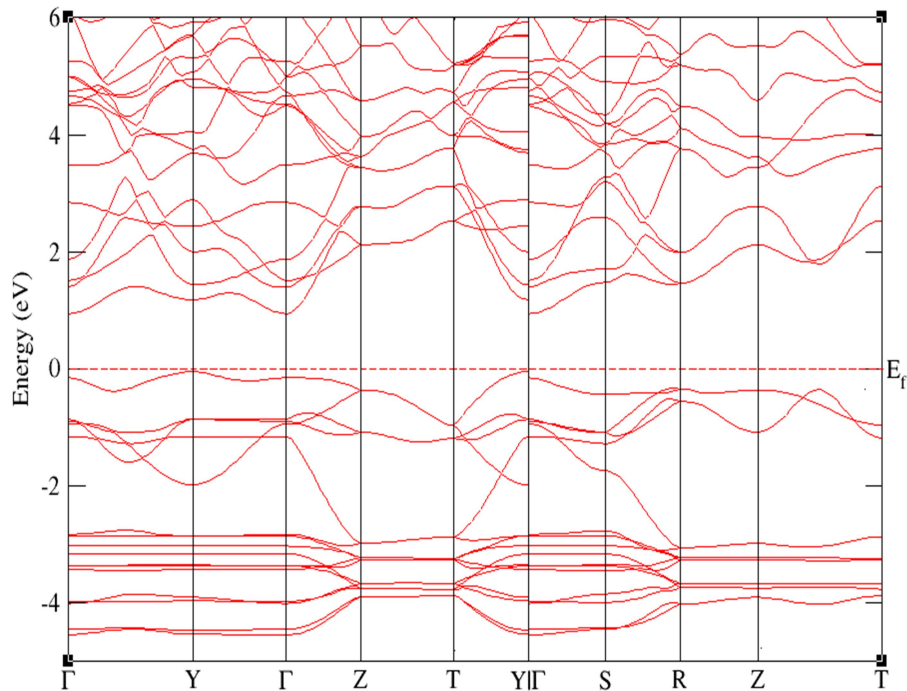
**Figure 16.5:** The computed energy band structures of ternary pnictides K2SbAu

The figure depicts band spectra of the compound under study, using generalized gradient approximation (GGA) along high symmetry Brillion zone points. Where the level of Fermi energy was set at zero, as shown by the dotted line from the band structure(Tran and Blaha, 2009). The illustrated level is composed of occupied valence bands of K2SbAu, while the one above the fermi level consists of unoccupied conduction bands. The electronic bandgap for the K_2SbAu compound using GGA was found to be 0.943eV. We did a comparison using Local density Approximation and obtained similar band spectra of the material as shown.
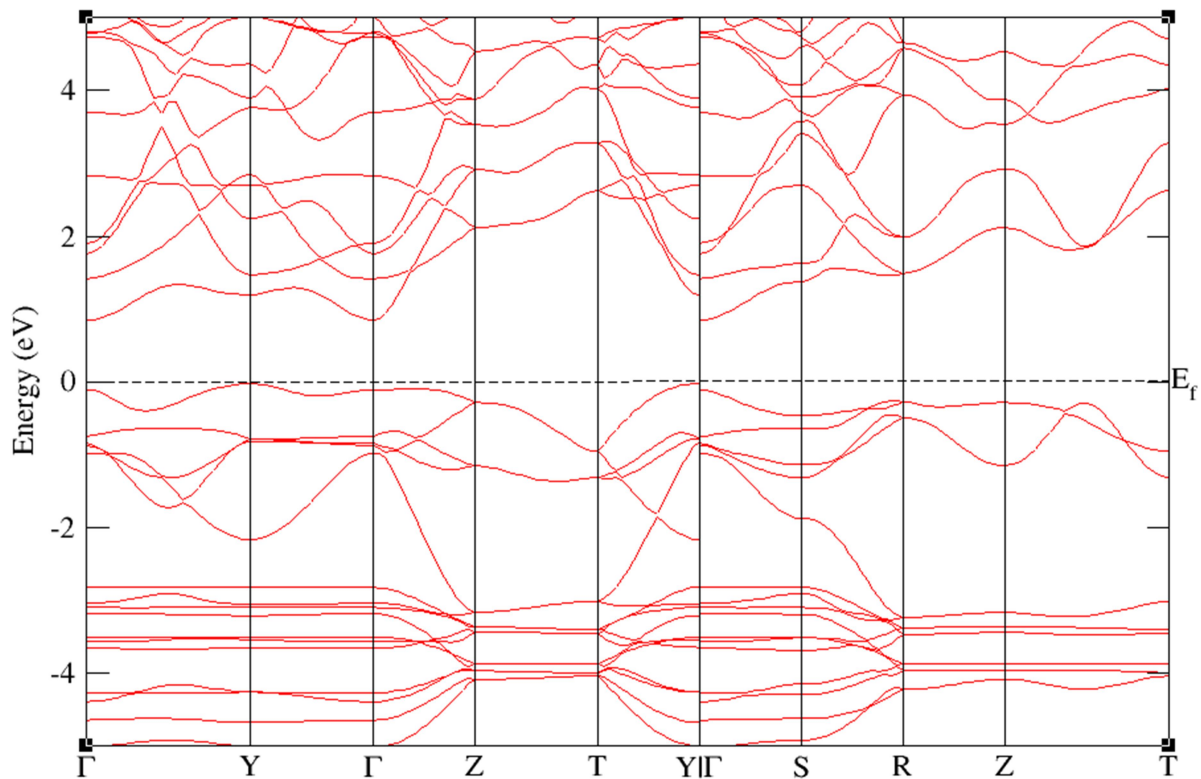
Figure 17.5: Calculated band spectra using LDA

While for LDA the gap energy is 0.848166eV; the deviation is a result of the underestimation of values for Local Density Approximation for this compound. The compound K2SbAu is of semiconducting nature having a direct band for the three approximations. Another comparison was done using a newly generated functional known as PBEsol, since the ternary pnictide material under study is stable we again obtain a similar band structure computationally as indicated in the diagram below.

Figure 18.5: Calculated band spectra using PBEsol functional
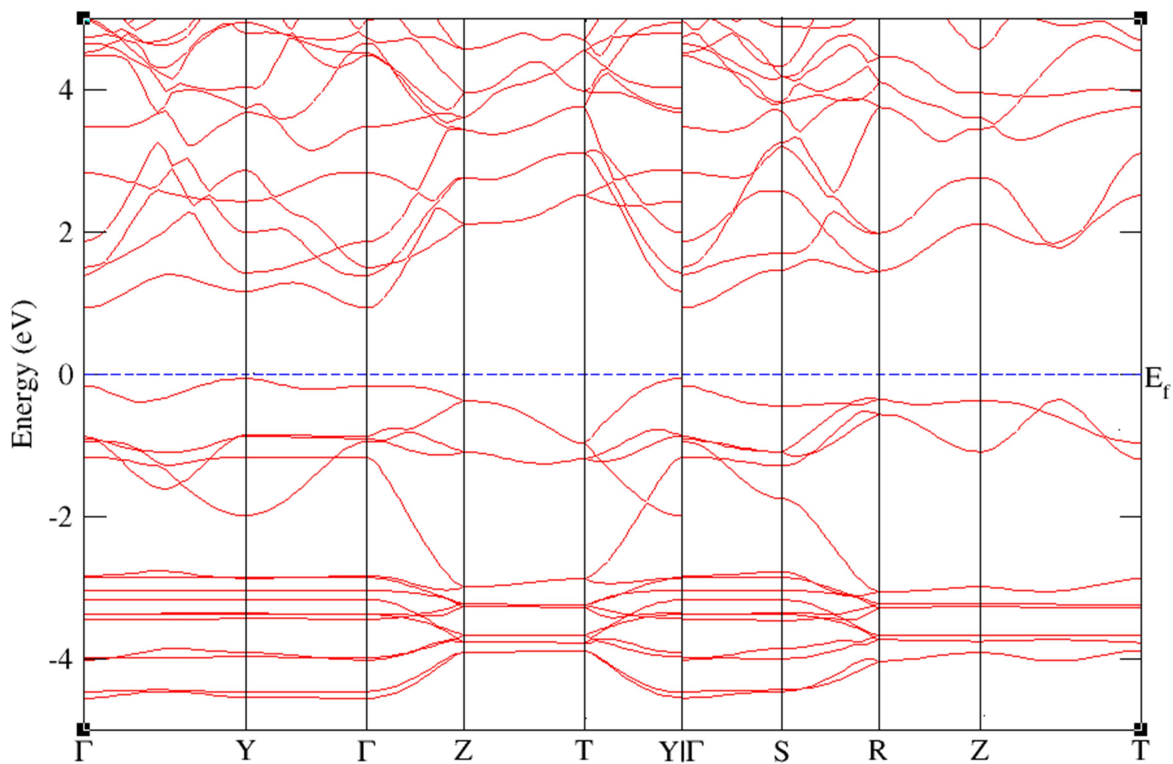
Similarly, structure's band plotted and density of state was computed. The band gap obtained was 0.906 eV a value close to pseudopotentials for GGA+PBE.

**Table 5.5**: calculated electronic band gap of the K_2SbAu for various approximations.

Method	GGA	PBEsol	LDA
Band gap (eV)	0.9430	0.9060	0.8482

With optimized lattice constants in this work, the band structure of the studied material which is a result of Kohn-Sham was deduced with the use of PBEsol, LDA and PBE functional along high symmetry points. From the three methods, the valence band maximum (VBM) and conduction band were calculated within the gamma point of the Brillouin zone. Thus from the research investigated, the material has a direct band gap semiconductor character at the gamma point. In the three functional, the fermi level was shifted to zero hence closer to the VB indicating a p-type semiconductor(Yin *et al*., 2014). Our calculated band gaps are tabulated hence, it is clear the band gap is 0.9430, 0.9060 and 0.8482eV for various approximations used.

However, the experimental band gaps have not yet been reported, thus in comparison to materials of the same stoichiometry, we found that the material predicts an agreement with it. The difference is a result of different functions used during computations. LDA thus underestimated the bandgap. The solution to this problem is the use of hybrid functionals or a many-body approach, with an increase in the computational demanding
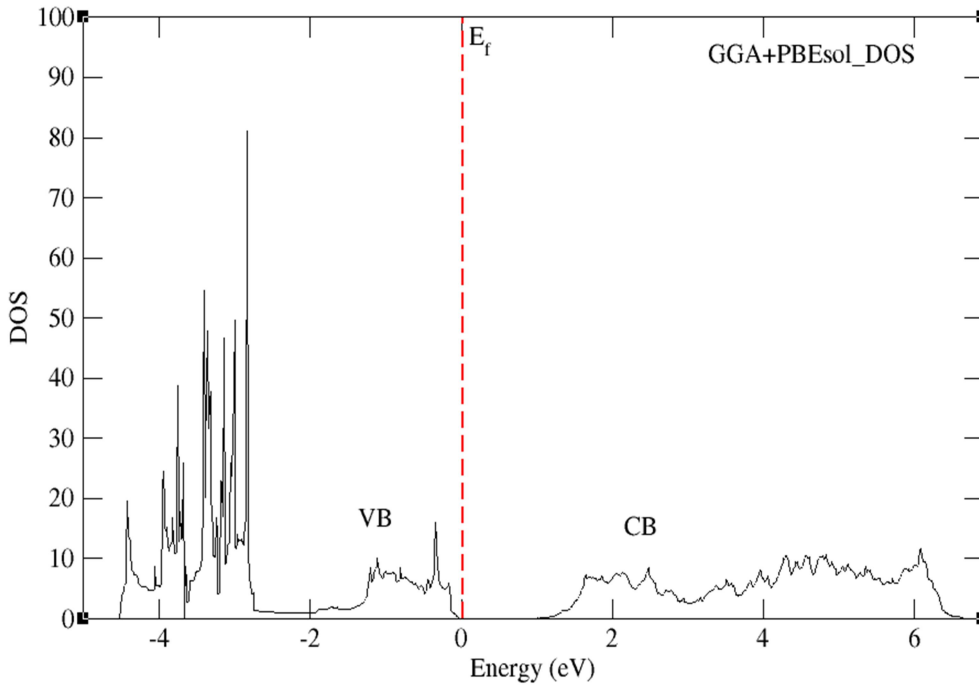
5.1.9 Density of States

The electron probability distribution in the energy spectrum is known as the Density of states (DOS)(Yin *et al*., 2014). Figure 17 shows how the total density of states for the investigated structure using PBE, PBEsol and LDA functional. It can be seen that indeed the contribution is around the fundamental band gap contributed by the elements of material compound K, Sb, and Au as seen from the plot(Tran and Blaha, 2009). The Fermi level was set at zero being closer to valence bands. Using generalized gradient approximation functional(GGA)(Perdew *et al*., 1996), we computed the DOS of the studied material.
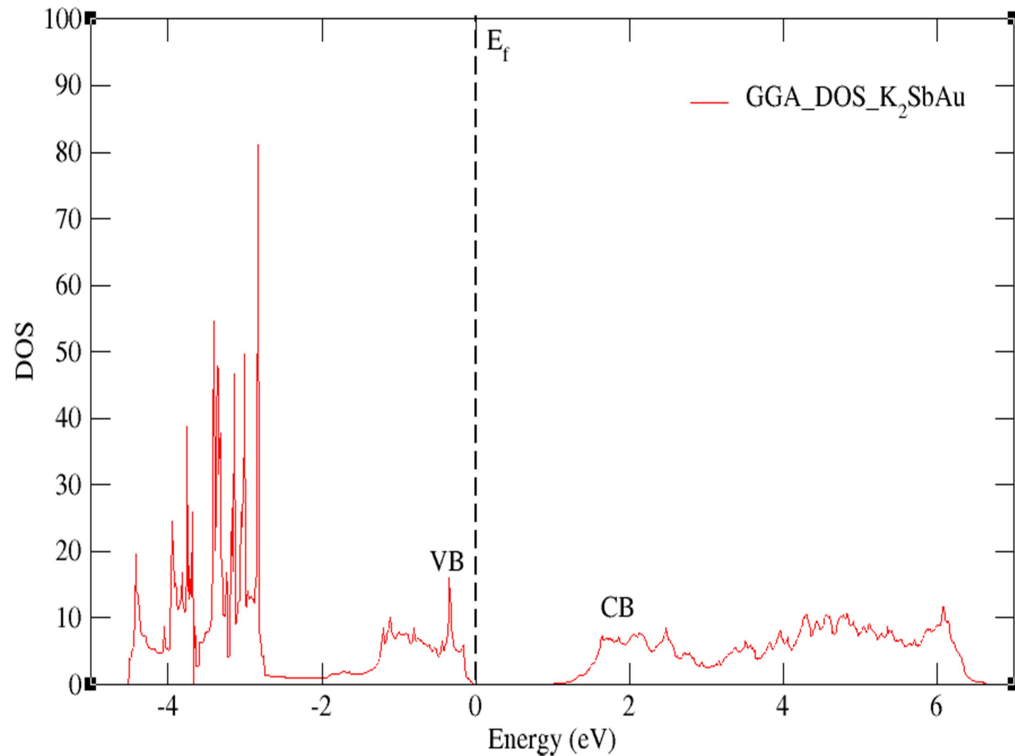
**Figure 19.5:** Density of states (DOS) for PBE+GGA

The density of states reveals the valence band and conduction band separated by an energy gap hence this material is a p-type semiconductor compound since the fermi level is closer to the valence band VB. The Density of state is a variable quantity hence once manipulated can improve device performance. Momentum for electrons and photons in the density of states is calculated by counting up the states to a given wave number. This is determined from the number of waves confined to a box within a volume space

For the hybrid functional of PBEsol, the computed Dos structure was also obtained as shown in figure 18. It still shows a similar structure as for GGA, even though a different pseudopotential was used for the particular functional.

Figure 20.5: Density of states for PBEsol functional (Kim e*t al*., 2010)

Lastly, we applied similar computation technique using LDA functional to elucidate materials density of states, and obtained the results as plotted in figure **19**.
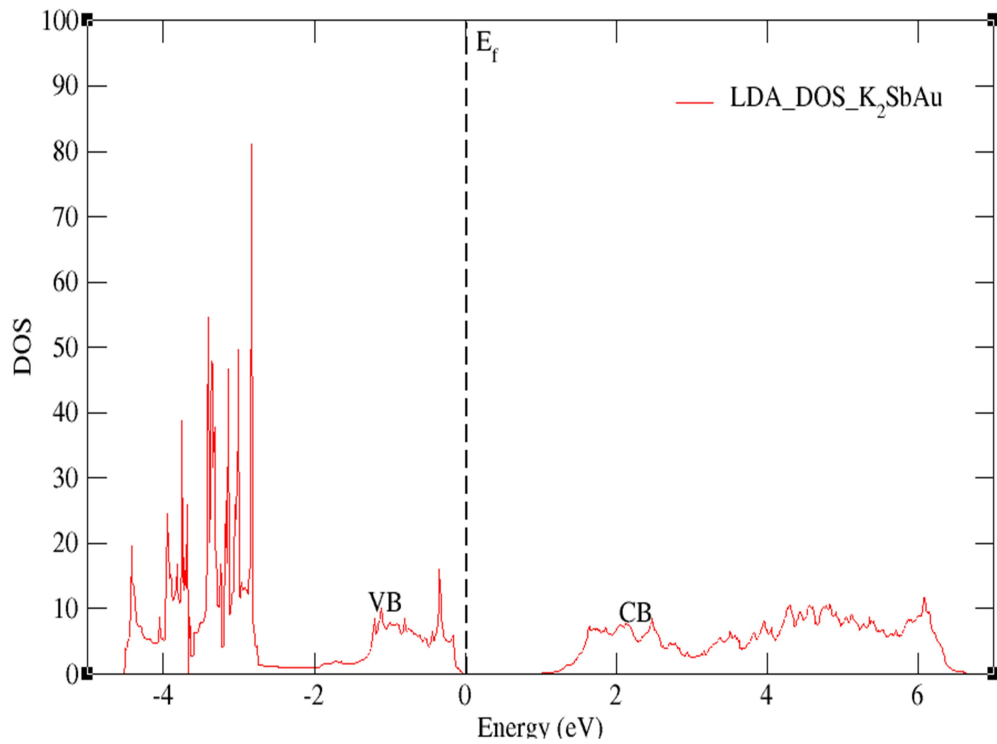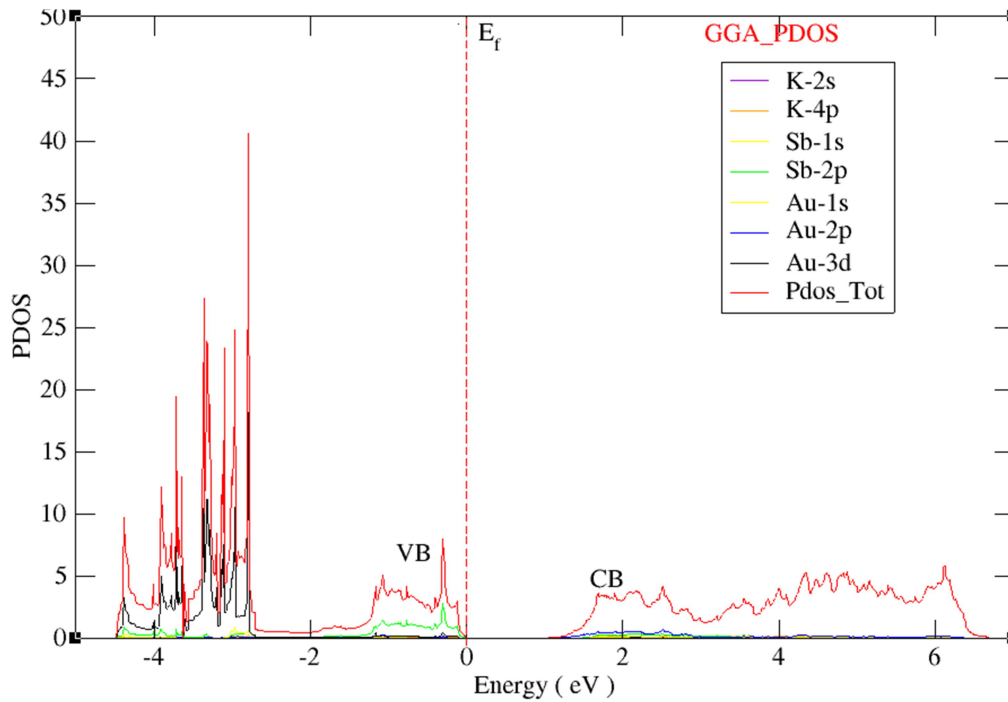
Figure 21.5: LDA Density of states

Since we are first reporting material properties theoretically, our point of a reference relied on compounds of similar ternary semiconductors like as referenced (Verma *et al.*, 2011) CuAlS2 depicts similar characteristics as K2SbAu.
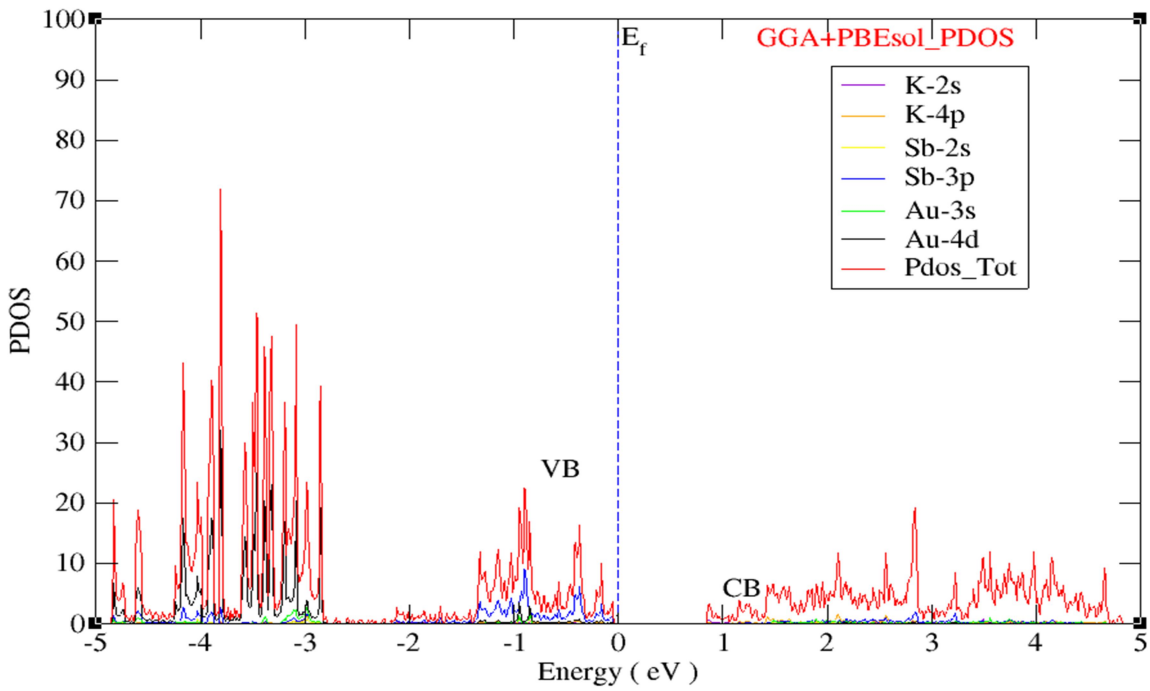
5.2.0 Projected density of state

From the total density of states, we again further studied materials PDOS as the last electronic properties for the three functional, their corresponding orbital contribution deduced,
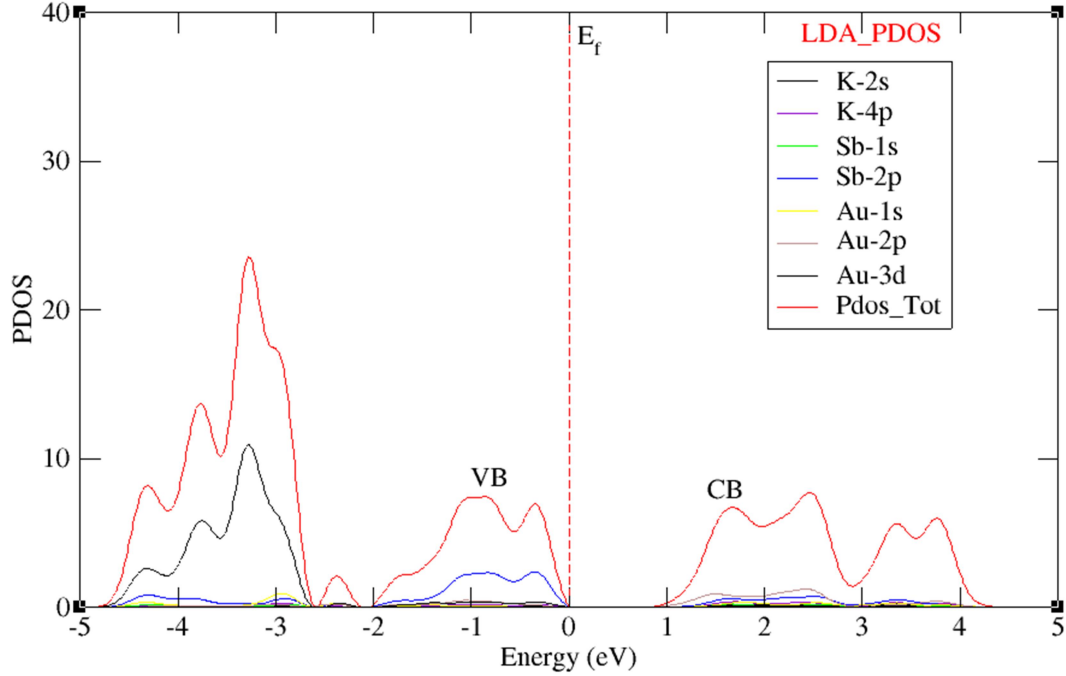

Figure 22.5: Projected density of states K2SbAu

The K_2SbAu has fermi energy nearer VB and hence is a p-type semi-conductor compound however the contrary was to be true if it was near CB hence becoming an n-type semiconductor

Figure 23.5: Electronic properties of projected density of states (PBEsol)(Kim *et al*., 2010)

Figure 24.5: LDA Projected density of states K2SbAu.
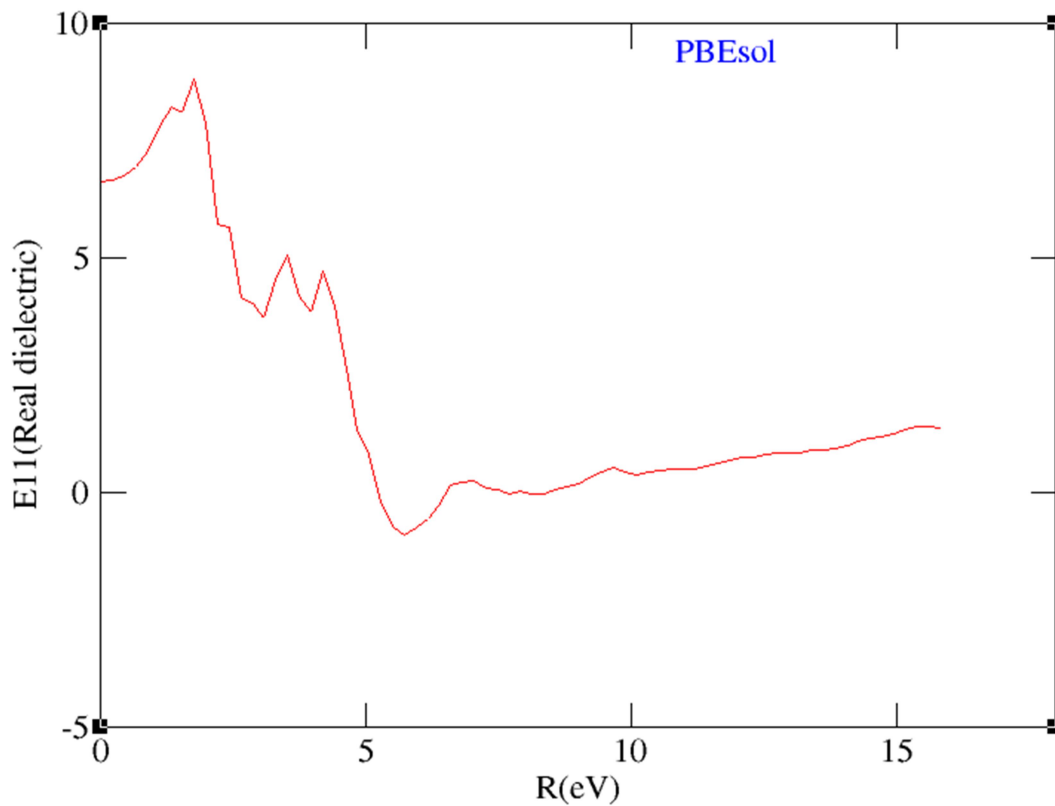
5.2.1 Optical Properties of K2SbAu

Calculated optical properties of K_2SbAu at equilibrium lattice constant were obtained as shown in the figures. This is achieved by the use of functional, in this work, PBE, PBEsol and LDA functional are used to obtain optical spectra when it is at the stable lattice constant. In Fig22 (a), b indicates the computed imaginary constant of dielectric denoted as $\varepsilon_2(\omega)$ and real ε_1 of the dielectric constant for K_2SbAu for radiation up to 25 eV. The function denoted as $\varepsilon_2(\omega)$ shows an imaginary dielectric constant that exhibits one peak.

These occur as results of orbital contribution in direct optical transition using the states of valence in its valence band and conduction band. The real dielectric ε_1 in the limit of zero energy is equal to the square of refractive index n. From Fig 23 the obtained value of the refractive index n is 2.4 eV which is in excellent agreement with the experimental value of 2.0–2.5 eV of similar compounds like CuAlS2(Kim *et al*., 2010).

Fig. 24 shows the loss function of K_2SbAu. The loss of energy for electrons is an important factor in describing the energy loss of a fast electron traversing in the material. The prominent

peak in loss function L (ω) spectra located at 11.43 eV represents the characteristic associated with the plasma resonance and the corresponding frequency is the so-called plasma frequency. Fig. 25 displays the reflectivity of K_2SbAu. The peak of L(ω)in Fig. 24 corresponds to the trailing edges of the reflection spectra in Fig. 25. For instance, the prominent peak of the energy loss function L(ω) located at 11.43 eV corresponds to the abrupt enhancement of R(ω)(Mbilo *et al*., 2022). The purpose of such properties is to help in photovoltaic devices since it is very vital to determine the region of higher conductivity. Figure 26 indicates a higher peak of conductivity. The curve for conductivity relates to the imaginary part of the dielectric function $\varepsilon_2(\omega)$. Graphical plot for real and imaginary dielectric plots as indicated for Peso.

Using dielectric constants known as real and $\varepsilon_{im}(\omega)$ imaginary tensor, we compute the absorption spectra α(ω), energy loss L(ω), refractive index n(ω) and reflectivity(Taylor et al., 2013). According to knowledge present on this compound, it is the first time to study the optical properties of K_2SbAu ternary semiconductor. The PBEsol approximation was used and the results obtained for various optical properties is as shown below (Pilania and Sharma, 2013)

**Figure 25.5:** Calculated real dielectric constant for optical properties (Kim *et al*., 2010)
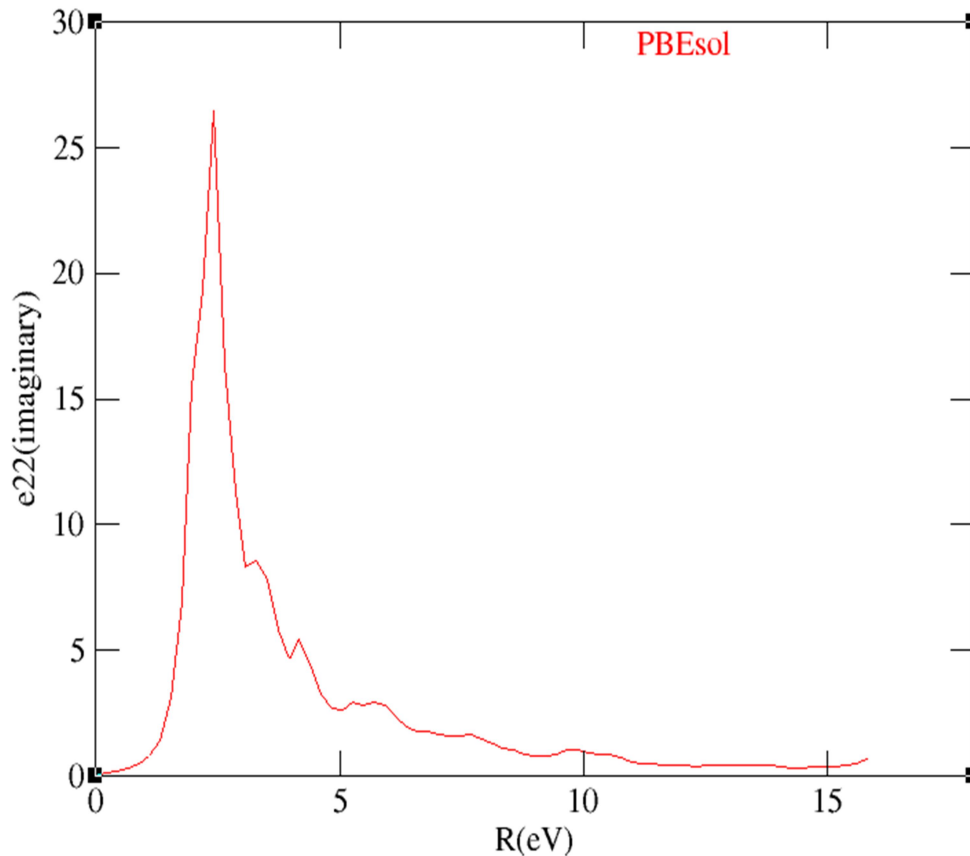
Figure26.5: showing the imaginary $\varepsilon_2(\omega)$ plot for K_2SbAu PBEsol

The material's response to such properties depends on the nature of the medium which is described by the energies of photons ingrained by the function $\varepsilon(\omega)$ (Mbilo *et al.*, 2022). The dispersion of light is attributed to the real part dielectric constant $\varepsilon(\omega)$ and demonstrated by the refractive index; whereas absorption of light in the medium relies on the imaginary part and is embedded in the absorption coefficient(Pilania and Sharma, 2013).

In order to design a good optoelectronic device, we need a more accurate idea of refractive indices. The measure of material transparency to the incident photons is known as the refractive index, which is considered an important physical parameter for semiconductor materials. It is because of its close relation to the band structure and electronic properties of semiconductor materials.
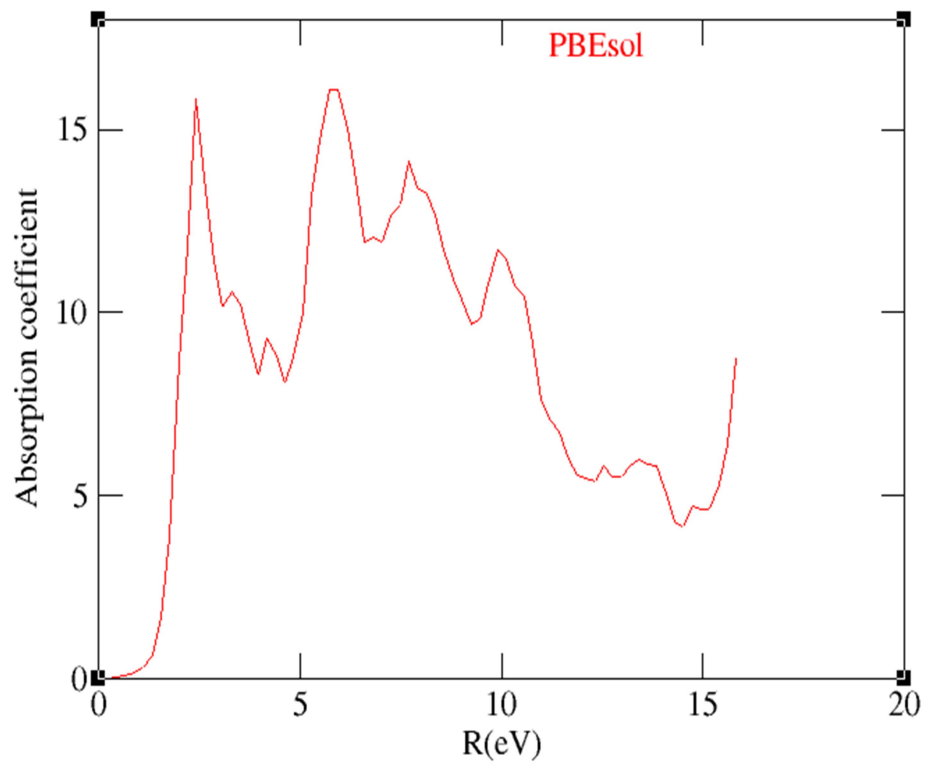
**Figure 27.5:** showing the absorption spectra **α (ω)** for PBEsol approximation
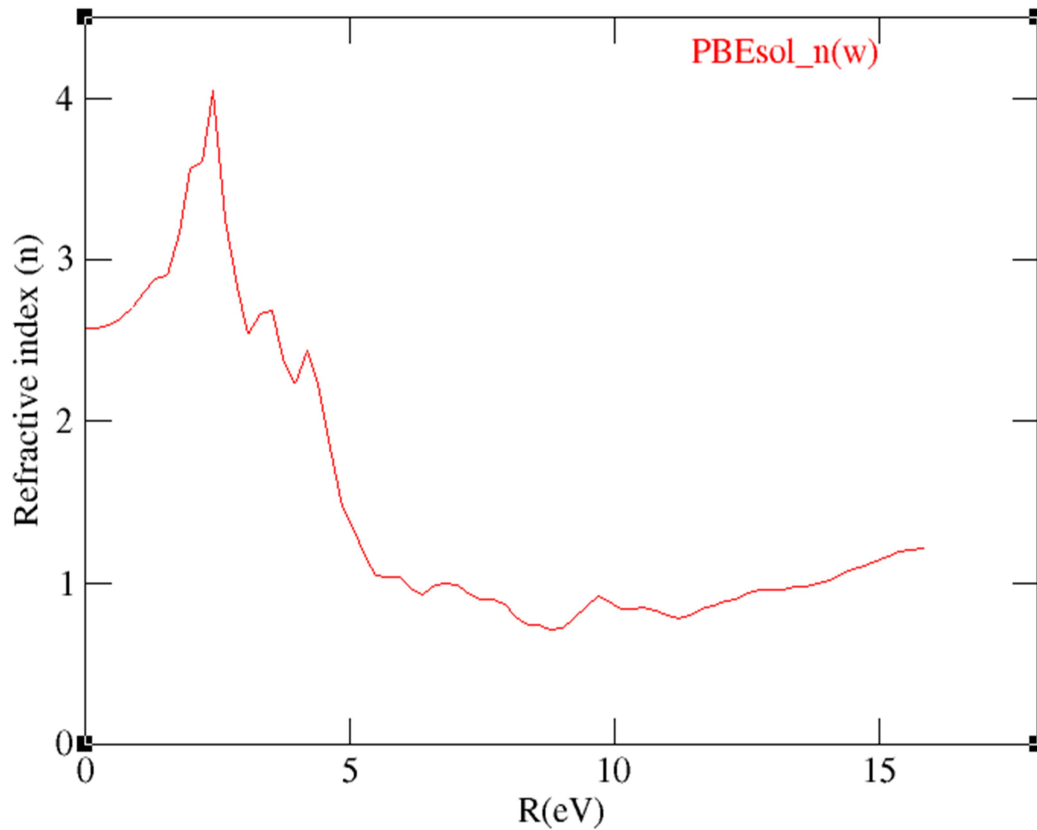
Figure28.5: calculated refractive index n (ω) optical properties

Apart from the refractive index, there exists another vital characteristic of the material known as reflectivity R(ω), which can be illustrated as the ratio of the reflected incident light power and describes the optical response of the surface of a material(Taylor *et al*., 2013). It has an inverse relation to the loss of energy function. From the calculated values of refractive index n(ω) and energy loss coefficient, we calculated the reflectivity of the material under study as shown.
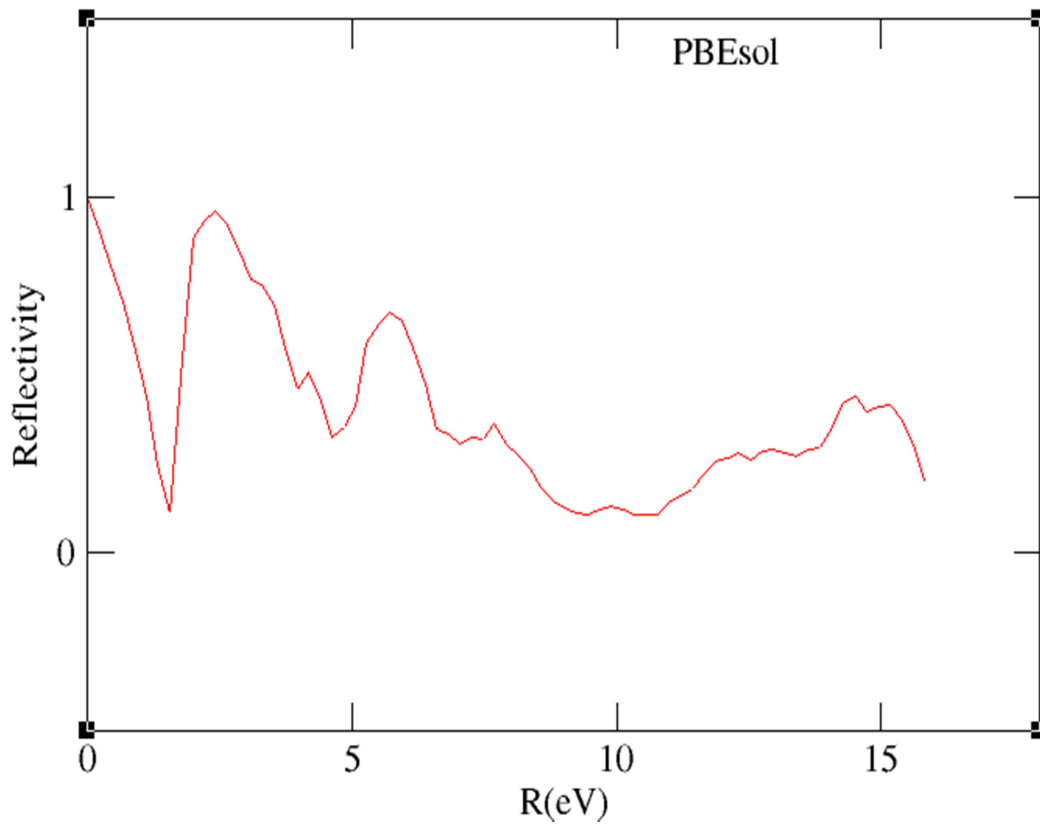
Figure 29.5: Calculated Reflectivity of the material K2SbAu
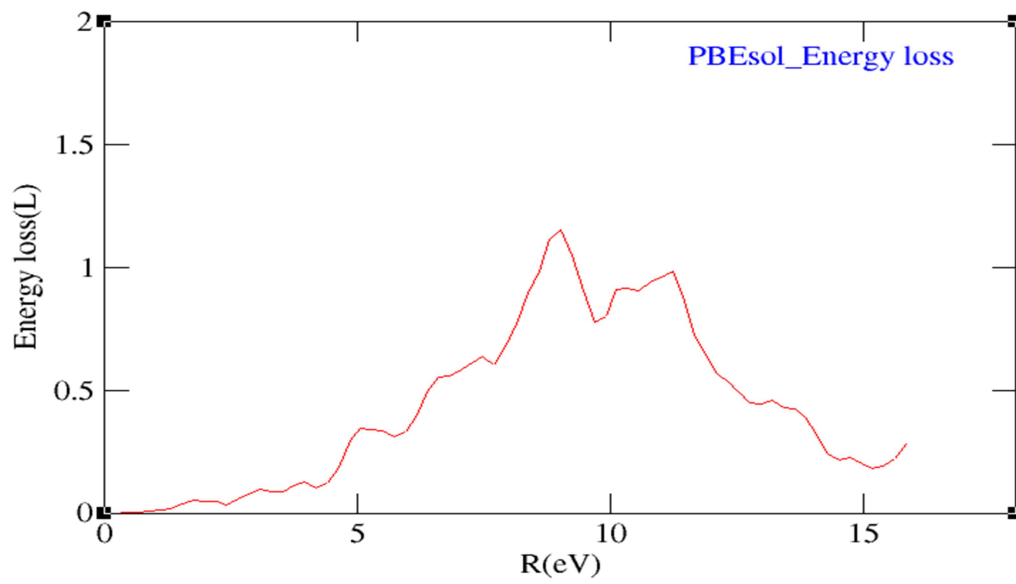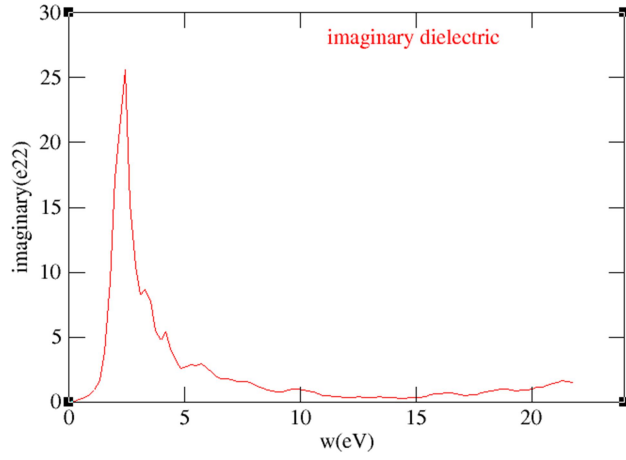

Figure 30.5: computed Energy loss coefficient optical property

Similar computation was performed for LDA functional, and the optical properties of the material obtained as shown in the figures,
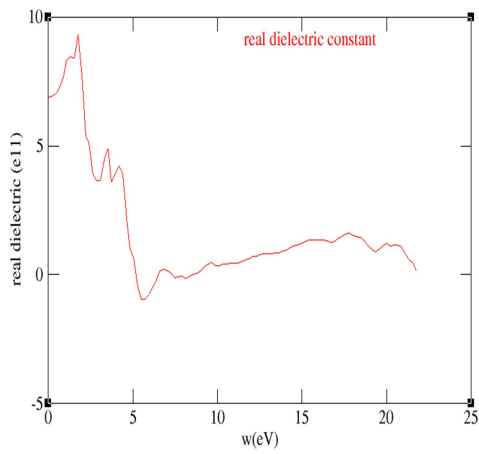
A   B

Figure 31.5, (A), calculated real dielectric constant while **figure 32.5:(B)** the imaginary dielectric for LDA
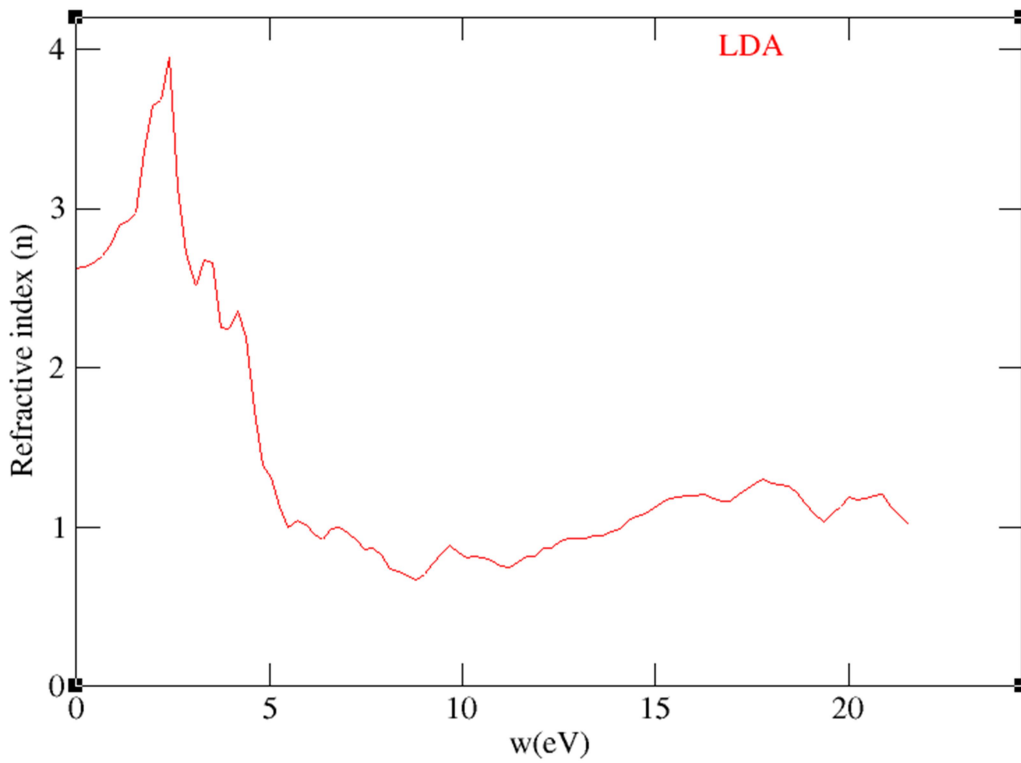
Figure33.5: Refractive index for LDA functional

C   **D**
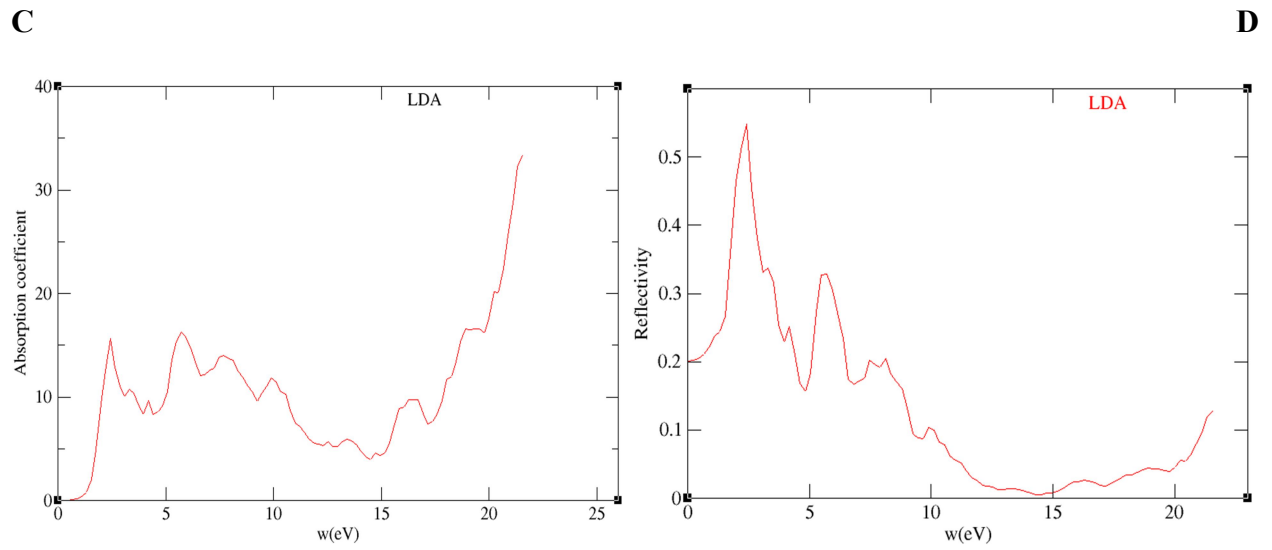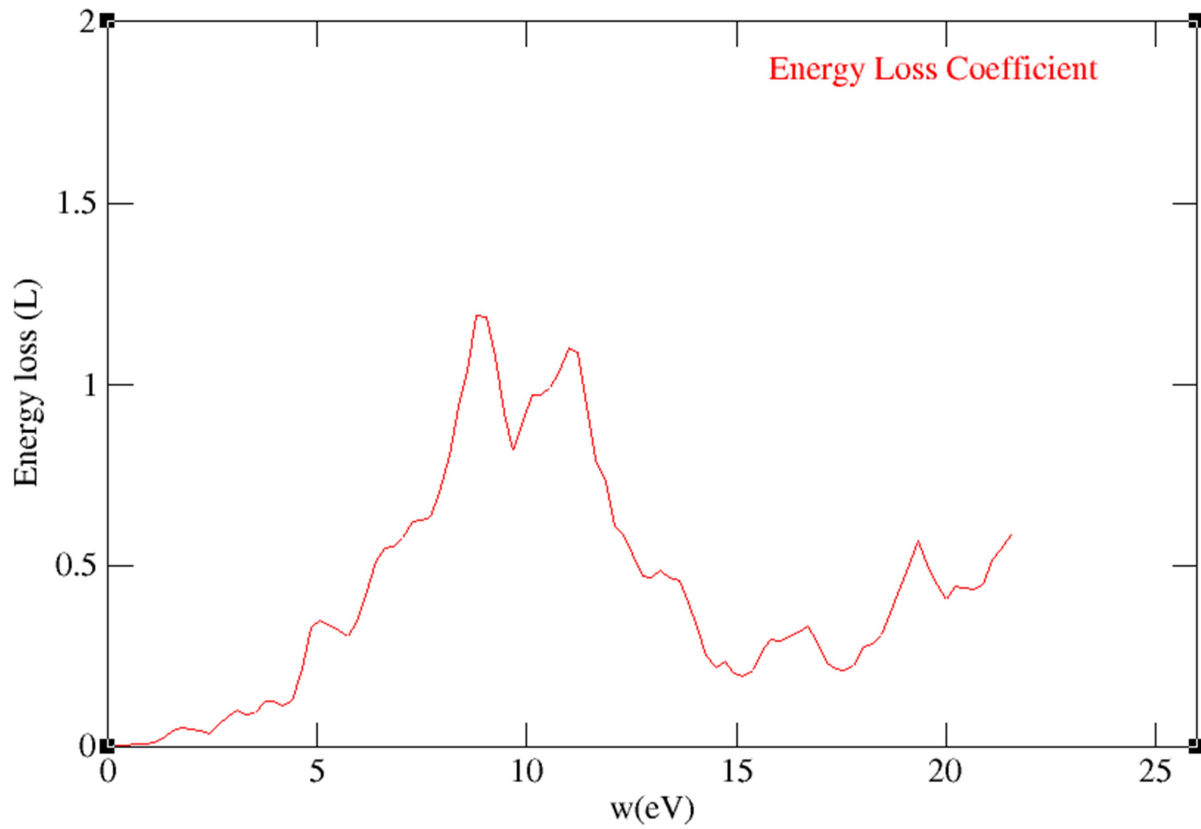

Figure **C**, indicates absorption coefficient of ternary semiconductor while **D** display Reflectivity.

Figure 34.5: shows computed LDA energy loss optical properties of ternary K2SbAu

The compound has also been interpreted for reflectivity as a function of energy from Figure D, from infrared regions to UV spectra region it has a similar trend as observed for absorption in Figure C(Irfan *et al.*, 2021). The coefficient of absorption is required to manufacture an efficient photovoltaic system, from the graphs the low absorption is from (0-2eV) and the medium occurs 5 to 15eV spin-up. The reflectivity has also an inverse relation to the energy loss function as indicated by the comparable plots(Irfan *et al.*, 2021).

For PBE+GGA functional, similar optical properties were obtained,
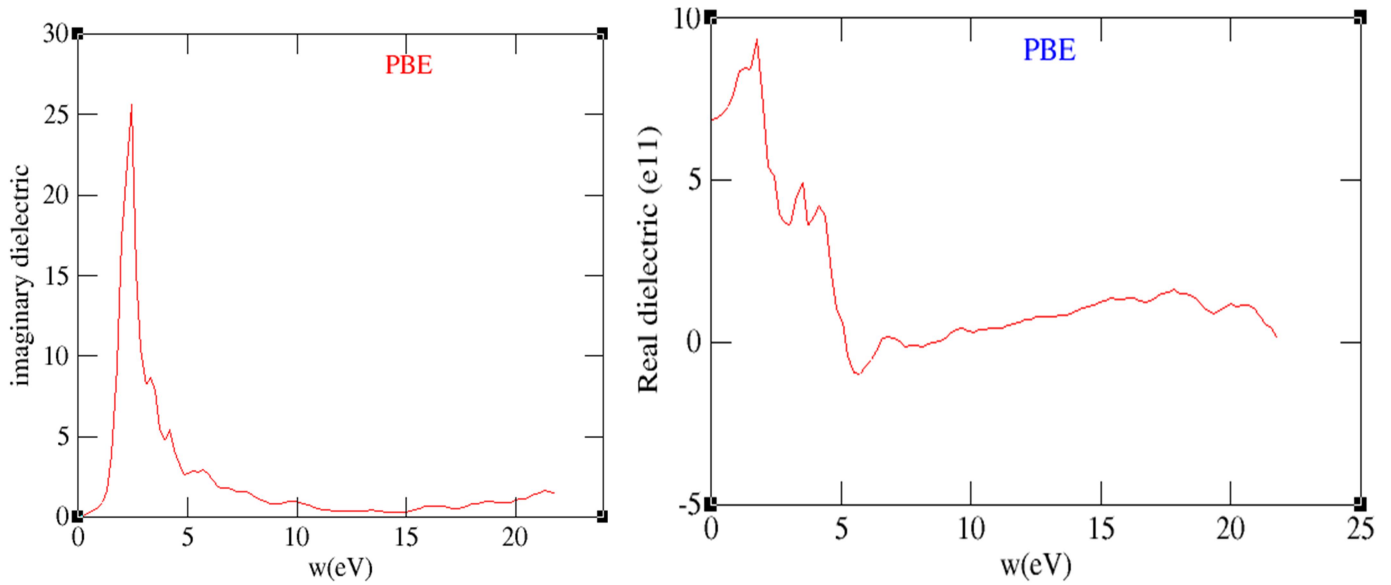
Figure 35.5 and **Figure36.5** respectively shows corresponding real and imaginary dielectric spectra for PBE.
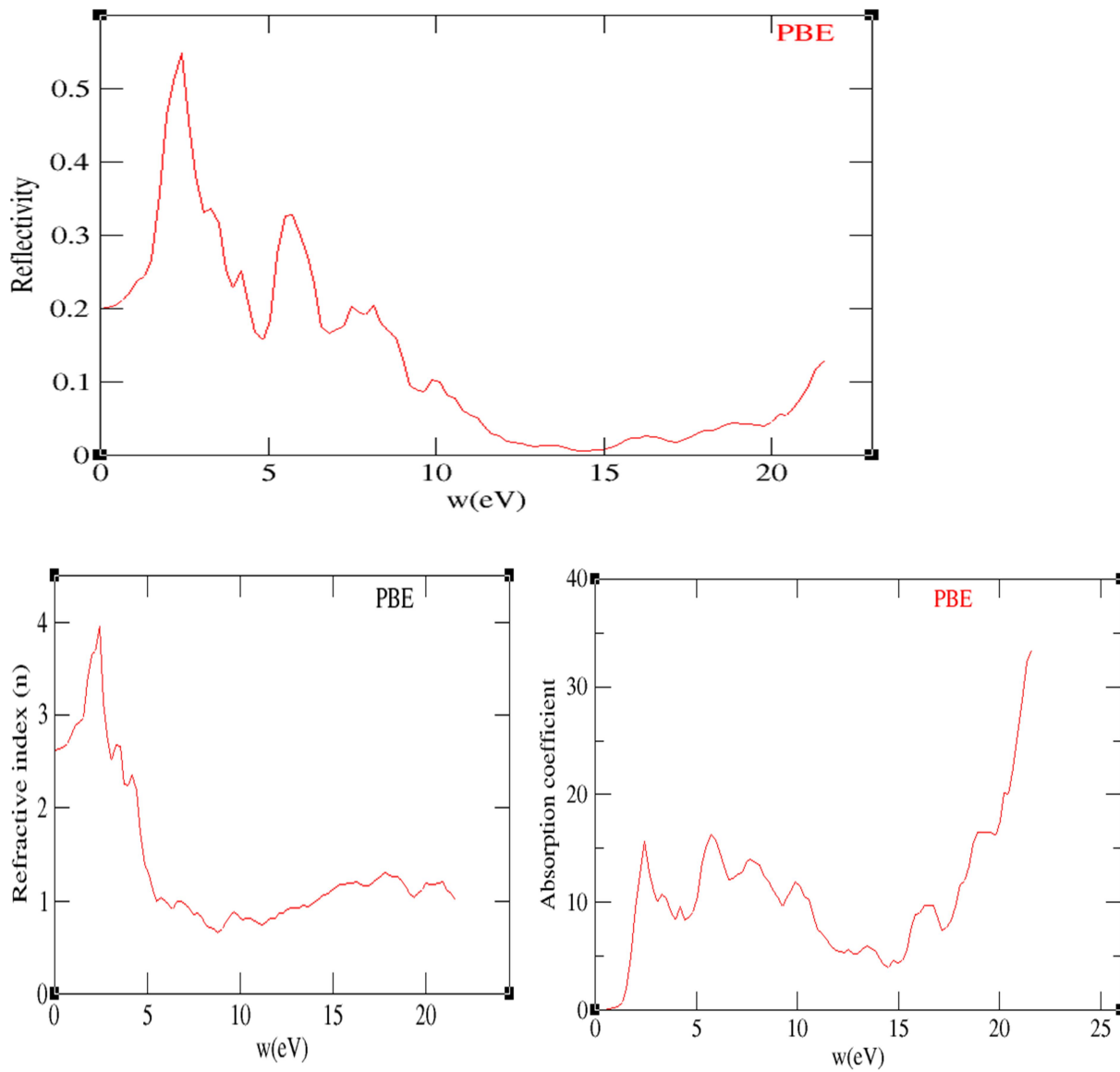
Figure 37.5: Refractive index and Absorption coefficient for pnictide ternary compound K2SbAu (PBE).

Figure 38.5: Energy loss coefficient of ternary compound for optical properties.

CHAPTER SIX: CONCLUSION AND RECOMMENDATIONS

6.1 CONCLUSIONS

In this thesis, structure, electronic, mechanical (physical) and optical properties were calculated on ternary pnictide semiconductor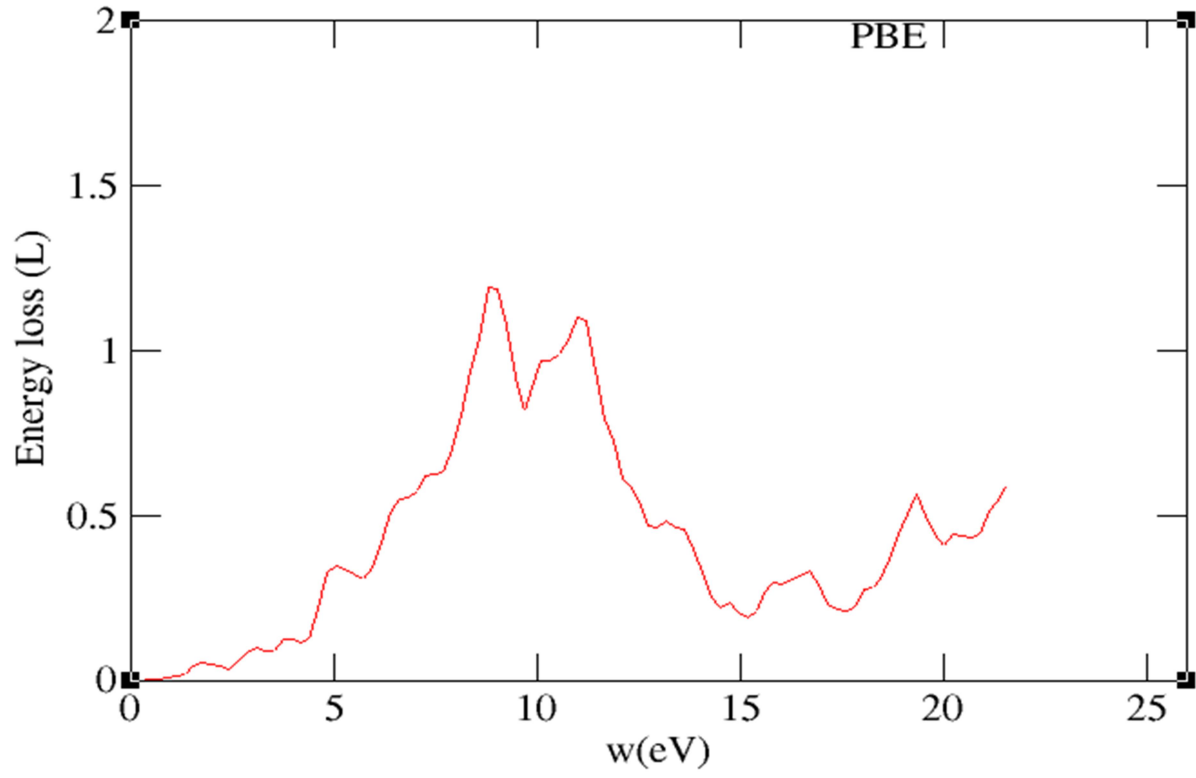 compound K_2SbAu. This was done using first-principles calculations from density functional theory in order to provide vital information for its application in optoelectronics. All structure optimizations and electronic structures such as band structure, the density of states and projected density of states were performed using the Quantum espresso code. The comparison was by use of three distinct functionals, that is PBE, PBEsol and LDA together with similar materials with the same stoichiometry. Our results are consistent in most cases with three functional applied and existing pnictide ternary compounds. We, therefore, hope our study would be paramount in providing better theoretical knowledge and an eye-opener for experimental research on this material.

The band gap values, total density states and projected density of states which are electronic properties were obtained at ground state, together with structural properties obtained from the computations of lattice parameters, bulk moduli, young modulus, Poisson ratio and shear moduli.

Results for elastic constants are in agreement with the three approximations functional used hence consistency is achieved. The Murnaghan third-order equation of state gives these ground state structural properties for PBE, PBEsol and LDA as obtained in chapter five 16.55 GPa,15.11 GPa and 12.62 GPa bulk moduli respectively. For shear moduli, 7.76 GPa, 7.80 GPa and 7.24 GPa respectively then lastly young moduli of 20.09 GPa, 19.95GPa and 18.15GPa were obtained. The K_2SbAu has a narrow band gap maximum being 0.9430eV which is direct, hence the material studied displayed properties of a p-type semiconductor as the fermi zero line was closer to valence band VB. Thus the majority of charge carriers are positive holes.

The elastic constants and structural stability are studied using PBE, PBEsol and LDA functional. The relaxed system is dynamically stable thus there are no negative values along the high symmetry Brillouin zone, thus satisfying all the mechanical stability criteria for the material crystal structure. Electronic properties were investigated by calculating the band structure, partial density of states (PDOS), and the total density of states (TDOS) using the PBEsol functional, PBE and LDA.

The coefficient of absorption is needed to manufacture an efficient photovoltaic system, from the graphs the low absorption is from (0-2eV) and the medium occurs 5 to 15eV spin-up. The reflectivity has an inverse relation to the energy loss function as indicated by the comparable plots.

Most importantly, the highest absorption peaks occur in the optical region and hence may be a potential material for solar photovoltaic applications. The results show that K_2SbAu has potential applications in solar cells due to its narrow band gap. An area for further research can be done.

6.2 Recommendations

From the computed electronic properties such as band gaps, DFT calculations underestimate these values hence in order to overcome this hindrance we recommend the use of the GGA+U pseudopotential even though they are computationally expensive. Other than that, uses of approaches that widen that band gap are applicable. Such approaches involve a method of self-interacting correction that removes the Hartree term. Similarly, in order to obtain a better result, calculations ought to involve hybrid functional to give better results specifically the band gaps. With proper and successful access to high-performance computing resources, these studies can effectively be carried out at minimal costs.

In summary, obtained computational results for K_2SbAu are recommended for use as optoelectronic devices like solar cells and photovoltaic cells due to their optical properties depicted by the pnictide ternary compound.

6.3 Future work

1. Experimental study of structural and electronic properties of K_2SbAu pnictide ternary semiconductor

2. Further study to be on Investigating the thermoelectric transport properties of the K_2SbAu from a combination of first-principle calculations and semi-classical Boltzmann transport theory

REFERENCES

Adachi, S. (2017). Iii-v ternary and quaternary compounds. *Springer Handbooks*, **2,** 319–48933. https://doi.org/10.1007/978-3-319-48933-9_30

Al., manjula et. (2016). Progress in solar PV technology: Research and achievement. *Structural Analysis of the Material Science*, **20**, 443–461. https://doi.org/10.1016/j.rser.2012.09.028

Ambrosch-Draxl, C., and Sofo, J. O. (2006). Linear optical properties of solids within the full-potential linearized augmented planewave method. *Computer Physics Communications*, **175**(1), 1–14. https://doi.org/10.1016/j.cpc.2006.03.005

Bell, G. R. (2018). Molecular Beam Epitaxy of Transition Metal Monopnictides. In *Molecular Beam Epitaxy*. Elsevier Inc.**2**(12). https://doi.org/10.1016/b978-0-12-812136-8.00001-3

Beloš, M. V., Abazovíc, N. D., Jakovljevíc, J. K., Jankóvic, I., Ahrenkiel, S. P., Mítric, M., and Comor, M. I. (2013). Influence of sulphide precursor on crystal phase of ternary I-III-VI 2 semiconductors. *Journal of Nanoparticle Research*, **15**(12). https://doi.org/10.1007/s11051-013-2148-6

Boublenza, D. E., Zaoui, A., Djermouni, M., Kacimi, S., Lekhal, A., and Drief, F. (2021). *Materials Science in Semiconductor Processing New 122 -materials for optoelectronic applications : An ab-initio comparison analysis*. **133**(May), 105949. https://doi.org/doi:10.1016/j.mssp.2021.105949

Kittle, W. (1996). *21 . Introduction solid state physics*. **29,** 230–300.

Chandra, J., and Kholiya, K. (2015). High pressure equation of state for solids. *High Temperatures - High Pressures*, **44**(4), 297–308.

Chen and Dongguo. (2013). *Mechanical , electronic and optical properties of multi-ternary semiconductor alloys Copyright Warning and Restrictions*. **59**(2), 133–1272. https://doi.org/https://doi.org/10.1063/1.105472

Chen, D., and Ravindra, N. M. (2019). Other Miscellaneous Semiconductors and Related Binary, Ternary, and Quaternary Compounds. *Semiconductors*, **10-9**(chapt, 465–545. https://doi.org/10.1007/978-3-030-02171-9_8

Daoud, S. (2019). Empirical prediction of thermal properties, microhardness and sound velocity of cubic zinc-blende ALN. *Semiconductor Physics, Quantum Electronics and Optoelectronics*, **22**(4), 404–409. https://doi.org/10.15407/spqeo22.04.404

Daoud, Salah, Bioud, N., and Lebga, N. (2019). Elastic and thermophysical properties of BAs under high pressure and temperature. *Chinese Journal of Physics*, **57**(4), 165–178. https://doi.org/10.1016/j.cjph.2018.11.018

Edition, S., Koch, W., and Holthausen, M. C. (2001). Wolfram Koch , Max C . Holthausen A Chemist ' s Guide to. In *Neural Networks* (**Vol. 3).** http://doi.wiley.com/10.1002/3527600043

Es-smairi, A., Fazouan, N., Joshi, H., and Houssine, E. (2022). Journal of Physics and Chemistry of Solids First-principles calculations to investigate electronic , optical , thermodynamic and thermoelectric properties of new Na 6 ZnX 4 (X = O , S , Se) ternary alloys. *Journal of Physics and Chemistry of Solids*, **160 (1-8)**(August 2021), 110305. https://doi.org/10.1016/j.jpcs.2021.110305

Fan, Q., Yang, J., Fan, Q., and Cheng, X. (2017). *Subject Category : Subject Areas : Author for correspondence : Prediction for electronic , vibrational and thermoelectric properties of chalcopyrite AgX (X = In , Ga) Te 2 : PBE + U approach*. **4**(10), 170750. https://doi.org/https://doi.org/10.1098/rsos.170750

Gidopoulos, N. I., and Gross, E. K. U. (2014). Electronic non-adiabatic states: Towards a density functional theory beyond the Born-Oppenheimer approximation. *Philosophical Transactions of the Royal Society A: Mathematical, Physical and Engineering Sciences*, **224**(1)(2011), 2013–0059. https://doi.org/10.1098/rsta.2013.0059

Guevara, H., Rodríguez, A. G., Navarro-Contreras, H., and Vidal, M. A. (2007). Nonlinear behavior of the energy gap in Ge1-x Snx alloys at 4 K. *Applied Physics Letters*, **91**(16), 16–19. https://doi.org/10.1063/1.2800296

Haase, M. A., Qiu, J., DePuydt, J. M., and Cheng, H. (1991). Blue-green laser diodes. *Applied Physics Letters*, **59**(11), 1272–1274. https://doi.org/10.1063/1.105472

Hao, S., Zhao, L., Chen, C., Dravid, V. P., Kanatzidis, M. G., and Wolverton, C. M. (2014).

Theoretical Prediction and Experimental Confirmation of Unusual Ternary Ordered Semiconductor Compounds in Sr − Pb − S System. **136** (1), 1628–1635. https://doi.org/https://doi.org/10.1021/ja411857y

Hill, R. (1952). The elastic behaviour of a crystalline aggregate. *Proceedings of the Physical Society. Section A*, **65**(5), 349–354. https://doi.org/10.1088/0370-1298/65/5/307

Irfan, M., Azam, S., & Iqbal, A. (2021). Proposal of new stable ABC2 type ternary semiconductor pnictides K3Cu3P2 and K3Ni3P2: First-principles calculations and prospects for thermophysical and optoelectronic applications. *International Journal of Energy Research*, **45**(2), 2980–2996. https://doi.org/10.1002/er.5992

Griffiths, D. (2000). Introduction to quantum mechanics.pdf. In *Journal of Catalysis* (**Vol. 193**, Issue 2, pp. 224–237). http://www.sciencedirect.com/science/article/pii/S0021951700928914

Jaffe, J. E., and Zunger, A. (1984). Electronic structure of the ternary pnictide semiconductors ZnSiP2, ZnGeP2, ZnSnP2, ZnSiAs2, and MgSiP2. *Physical Review B*, **30**(2), 741–756. https://doi.org/10.1103/PhysRevB.30.741

John, R. (2007). Tuning of Energy Band Gaps in Ternary Semiconductors. *Advanced Materials Research*, **31**(2), 164–166. https://doi.org/10.4028/www.scientific.net/amr.31.164

Kim, Y. S., Marsman, M., Kresse, G., Tran, F., and Blaha, P. (2010). Towards efficient band structure and effective mass calculations for III-V direct band-gap semiconductors. *Physical Review B - Condensed Matter and Materials Physics*, **82**(20), 1–11. https://doi.org/10.1103/PhysRevB.82.205212

Knauth, P. (2002). Erratum: Defect and transport properties of nanocrystalline ceramics and thin films (Journal of Solid State Electrochemistry (2002) 6 (165-171)). *Journal of Solid State Electrochemistry*, **6**(4), 290. https://doi.org/10.1007/s10008-002-0278-3

Kohn, S. (1995). Self-Consistent Equations Including Exchange and Correlation Effects. *Korean Journal of Physiology and Pharmacology*, **140**(5), 1–10.

Koitabashi, K., Ozaki, S., and Adachi, S. (2010). Optical properties of single-crystalline chalcopyrite semiconductor AgInSe2. *Journal of Applied Physics*, **107**(5), 1–11.

https://doi.org/10.1063/1.3309953

Kuykendall, T., Ulrich, P., Aloni, S., and Yang, P. (2007). Complete composition tunability of InGaN nanowires using a combinatorial approach. *Nature Materials*, **6**(12), 951–956. https://doi.org/10.1038/nmat2037

Madsen, G. K. H., and Singh, D. J. (2006). BoltzTraP. A code for calculating band-structure dependent quantities. *Computer Physics Communications*, **175**(1), 67–71. https://doi.org/10.1016/j.cpc.2006.03.007

Mahan, G., Sales, B., and Sharp, J. (1997). Thermoelectric materials: New approaches to an old problem. *Physics Today*, **50**(3), 42–47. https://doi.org/10.1063/1.881752

Mallmann, M., Niklaus, R., Rackl, T., Benz, M., Chau, T. G., Johrendt, D., Minár, J., and Schnick, W. (2019). Solid Solutions of Grimm–Sommerfeld Analogous Nitride Semiconductors II-IV-N2 (II=Mg, Mn, Zn; IV=Si, Ge): Ammonothermal Synthesis and DFT Calculations. *Chemistry - A European Journal*, **25**(69), 15887–15895. https://doi.org/10.1002/chem.201903897

Manfredi, G. (2020). Density functional theory for collisionless plasmas - Equivalence of fluid and kinetic approaches. *Journal of Plasma Physics*, **32**, 1–12. https://doi.org/10.1017/S0022377820000240

Martins, J. L., and Zunger, A. (1985). Binary vs ternary tetrahedra semiconductor. *Physical Review B*, **32**(4), 2689–2692. https://doi.org/http://dx.doi.org/10.1103/PhysRevB.32.2689

Mbilo, M., Manyali, G. S., and Musembi, R. J. (2022). *Ab Initio Study of K${_3}$Cu${_3}$P${_2}$ Material for Photovoltaic Applications*. **32**(April), 2–15. https://doi.org/10.1016/j.cocom.2022.e00726

McCandless, B. E. (2005). CdTe contacts for CdTe/CdS solar cells: Effect of Cu thickness, surface preparation and recontacting on device performance and stability. *Solar Energy Materials and Solar Cells*, **88**(1), 75–95. https://doi.org/10.1016/j.solmat.2004.10.010

Mokkapati, S., and Jagadish, C. (2009). III-V compound SC for optoelectronic devices. *Materials Today*, **12**(4), 22–32. https://doi.org/10.1016/S1369-7021(09)70110-5

Pan, A., and Zhu, X. (2015). Optoelectronic properties of semiconductor nanowires. In *Semiconductor Nanowires: Materials, Synthesis, Characterization and Applications*. Elsevier Ltd. https://doi.org/10.1016/B978-1-78242-253-2.00012-8

Payne, M. C., Teter, M. P., Allan, D. C., Arias, T. A., & Joannopoulos, J. D. (1992). Iterative minimization techniques for ab initio total-energy calculations: Molecular dynamics and conjugate gradients. *Reviews of Modern Physics*, **64**(4), 1045–1097. https://doi.org/10.1103/RevModPhys.64.1045

Perdew, J. P., Burke, K., and Ernzerhof, M. (1996). Generalized gradient approximation made simple. *Physical Review Letters*, **77**(18), 3865–3868. https://doi.org/10.1103/PhysRevLett.77.3865

Peter et al. (2005). Fundamentals of Semiconductors(Third edition). *Physics and Material Property*, **3**(57), 1–651. https://doi.org/https://doi.org/10.1103/PhysRevLett.77.3865

Pilania, G., and Sharma, V. (2013). First principles investigations of structural, electronic, elastic, and dielectric properties of KMgF3. *Journal of Materials Science*, **48**(21), 7635–7641. https://doi.org/10.1007/s10853-013-7581-5

Rogalski, A. (2005). HgCdTe infrared detector material: History, status and outlook. *Reports on Progress in Physics*, **68**(10), 2267–2336. https://doi.org/10.1088/0034-4885/68/10/R01

Scandolo, S., Giannozzi, P. I., Cavazzoni, C. I., de Gironcoli, S. I., Pasquarello, A. V., & Baroni, S. I. (2005). *First-principles codes for computational crystallography in the Quantum-ESPRESSO package Ab-initio calculations / Molecular dynamics / Phonons / Elasic constants / High-pressure / Quantum-ESPRESSO Computer program / Computational crystallography*. **220**, 574–579.

Schrödinger, E. (1926). An undulatory theory of the mechanics of atoms and molecules. *Physical Review*, **28**(6), 1049–1070. https://doi.org/10.1103/PhysRev.28.1049

Sheng, C. and, Xue, H. G., and Ping, G. and S. (2018). Multinary metal chalcogenides with tetrahedral structures for second-order nonlinear optical, photocatalytic, and photovoltaic applications. *Coordination Chemistry Reviews*, **368**, 115–133. https://doi.org/10.1016/j.ccr.2018.04.014

Shiyou, C. and, Gong, X. G., Walsh, A., and Wei, S. H. (2009). Electronic structure and stability of quaternary chalcogenide semiconductors derived from cation cross-substitution of II-VI and I-III-VI2 compounds. *Physical Review B - Condensed Matter and Materials Physics*, **79**(16), 1–10. https://doi.org/10.1103/PhysRevB.79.165211

Sholl and steckel. (2011). Density functional theory. *Electrocatalysis: Computational, Experimental, and Industrial Aspects*, **2**(1), 117–138. https://doi.org/10.1201/9781420045451

Skelton, J. M., Tiana, D., Parker, S. C., Togo, A., Tanaka, I., and Walsh, A. (2015). Influence of the exchange-correlation functional on the quasi-harmonic lattice dynamics of II-VI semiconductors. *Journal of Chemical Physics*, **143**(6). https://doi.org/10.1063/1.4928058

Snyder, G. J., and Ursell, T. S. (2003). Thermoelectric efficiency and compatibility. *Physical Review Letters*, **91**(14), 148301/1-148301/4. https://doi.org/10.1103/PhysRevLett.91.148301

Spohn, H., and Teufel, S. (2001). Adiabatic decoupling and time-dependent Born-Oppenheimer theory. *Communications in Mathematical Physics*, **224**(1), 113–132. https://doi.org/10.1007/s002200100535

Sturge, M. D. (2020). Electrons and Holes in Semiconductors. *Statistical and Thermal Physics*, **20**(1), 269–290. https://doi.org/10.1201/9781315275529-19

Moustakas. (1992). wider Band Gap semiconductor. *Materia Japan*, **242**(5), 371–379. https://www.jstage.jst.go.jp/article/materia1994/45/5/45_5_371/_pdf

Taylor, P., Miller, A., Miller, D. A. B., and Smith, S. D. (2013). Advances in Physics Dynamic non-linear optical processes in semiconductors. *Advances in Physics*, **6**(July 2013), 37–41.

Tran, F., and Blaha, P. (2009). Accurate band gaps of semiconductors and insulators with a semilocal exchange-correlation potential. *Physical Review Letters*, **102**(22), 5–8. https://doi.org/10.1103/PhysRevLett.102.226401

Verma, U. P., Jensen, P., Sharma, M., and Singh, P. (2011). Ab initio studies of structural, electronic, optical and thermal properties of CuAlS2 chalcopyrite. *Computational and Theoretical Chemistry*, **975**(1–3), 122–127. https://doi.org/10.1016/j.comptc.2011.03.008

Yang, J. (2005). Potential applications of thermoelectric waste heat recovery in the automotive industry. *International Conference on Thermoelectrics, ICT, Proceedings*, **2005**, 170–174. https://doi.org/10.1109/ICT.2005.1519911

Yin, W. J., Shi, T., and Yan, Y. (2014). Unusual defect physics in CH3NH3PbI3 perovskite solar cell absorber. *Applied Physics Letters*, **104**(6), 200–500. https://doi.org/10.1063/1.4864778

Yousuf, S., and Gupta, D. C. (2019). Thermoelectric response of ZrNiSn and ZrNiPb Half-Heuslers: Applicability of semi-classical Boltzmann transport theory. *Results in Physics*, **12**(October 2018), 1382–1386. https://doi.org/10.1016/j.rinp.2019.01.026